1981

Indirect estimation of parameters in a flexible tube, pulsatile flow system

Timothy Arthur Gray
Iowa State University

GRAY, TIMOTHY ARTHUR

INDIRECT ESTIMATION OF PARAMETERS IN A FLEXIBLE TUBE, PULSATILE FLOW SYSTEM

Iowa State University PH.D. 1981

Indirect estimation of parameters in a flexible tube, pulsatile flow system

by

Timothy Arthur Gray

A Dissertation Submitted to the
Graduate Faculty in Partial Fulfillment of the
Requirements for the Degree of
DOCTOR OF PHILOSOPHY

Department: Engineering Science and Mechanics
Major: Engineering Mechanics

Approved:

Signature was redacted for privacy.

In Charge of Major Work

Signature was redacted for privacy.

For the Major Department

Signature was redacted for privacy.

For the Graduate College

Iowa State University
Ames, Iowa

1981

TABLE OF CONTENTS

NOMENCLATURE

A	Lumen area of tube
A_o	Lumen area at pressure p_o
A_1	Lumen area of stenosis
A_p, A_d, A_b	Nominal lumen areas of proximal, distal and branch tubes
$\underline{b}$	Parameter vector
C	Vessel compliance per unit length
C_1, C_2	Empirical coefficients in linear compliance model
C_p, C_d, C_b	Compliances for proximal, distal and branch tubes
C_T	Lumped terminal compliance
c	Wavespeed of pressure pulse
D	Lumen diameter of tube
D_o	Lumen diameter at pressure p_o
D_1	Lumen diameter of stenosis
E	Vessel hoop modulus of elasticity
h	Vessel wall thickness
K_v, K_t, K_u	Empirical coefficients in stenosis pressure drop equation
(k)	Iteration number
$[K_1]$,$[K_2]$,$[K^e]$	Coefficient matrices in finite element approximation
L	Fluid inertance
L_s	Stenosis length
L_p, L_d	Distance to stenosis from proximal or distal tube end
L^e	Element length
$[M]$	Coefficient matrix in finite element approximation
N_i, N_j	Shape functions

$[N]$	Shape function matrix
p	Pressure
p_o	Nominal pressure, mean pressure
p_i, p_j	Nodal pressures
p^e	Element interpolation for pressure
Q	Flow
Q_i, Q_j	Nodal flows
Q^e	Element interpolation for flow
R	Resistance
R_1, R_2	Lumped peripheral resistances
R_o	Vessel lumen radius at pressure p_o
r_c, r_m	Residual error for continuity and momentum equations
S	Sum of squared error
t	Time
V	Volume of branch
v	Velocity
$[X]$	Sensitivity coefficient matrix
x	Axial position in vessel
$\underline{Y}$	Measured data vector
$\underline{y}$	Model response vector
Z	Peripheral resistance
Z_d, Z_b	Peripheral resistance for distal or branch tube
α	Frequency parameter
β	Empirical coefficient in compliance model
$\underline{\delta}$	Vector of nodal degrees of freedom

$\underline{\delta}^e$	Element vector of nodal degrees of freedom
δ_{mn}	Kronecker-δ
λ	Ratio of average squared velocity to squared average velocity
μ	Fluid viscosity
ρ	Fluid density
τ_o	Wall shearing stress
ψ	Seepage per unit length of vessel
ω	Natural (circular) frequency of pulsatile flow

CHAPTER 1

INTRODUCTION

Quantitative analysis of the human cardiovascular system has been the aim of much recent research. This research not only is of importance from an academic point of view, but also carries the possibility of providing clinical diagnostic tools for the assessment and treatment of circulatory disorders. However, the evaluation of important parameters of the circulation is hampered by the difficulty in obtaining accurate and reliable in vivo data. Moreover, some system parameters such as those associated with vessel elasticity and geometry are not readily accessible to direct measurement.

Recent advances in noninvasive measurement techniques such as the use of ultrasound and computer imaging techniques offer the promise of obtaining in vivo data with little or no effect upon the system. However, the question remains as to how such data can be put to use in determining parameters which cannot be measured directly.

Techniques for obtaining parameters indirectly from measured data are generally referred to as parameter estimation techniques. In a typical application, experimental data are utilized in conjunction with a mathematical model of the system under consideration to obtain estimates of unknown system parameters. An example is the determination of the slope and intercept of a linear model by the use of linear regression analysis. More generally, the mathematical model consists of a set of differential equations for which the measured data provide values of the response or state variables. For example, the parameters

of interest may appear as undetermined constants, initial conditions or boundary conditions. Parameter estimation techniques are based on the systematic variation of these unknown coefficients to minimize the error between the measured data and the response computed from the model.

The successful determination of the parameters of interest requires several ingredients. First, a mathematical model must be formulated which is capable of simulating measurable data and whose response is sensitive to the desired parameters. Second, some means must be available for accurately obtaining the necessary data from the physical system. Third, a performance index must be determined which portrays the error between the model and experimental response. Finally, a technique must be developed which will systematically vary the desired parameters to minimize the error.

The objective of this thesis is to apply the concept of parameter estimation to the study of the cardiovascular system. Specifically, the technique is used to determine pertinent system parameters related to blood flow through normal and diseased arterial segments. In accordance with the four required steps noted above, the following procedure has been followed.

First, a mathematical model of pulsatile flow in flexible tubes is developed which includes the effects of branching and a localized constriction. The medical term for such a constriction is a stenosis. The state variables of the model are pressures and flows calculated at a series of points in the tube. Second, an <u>in vitro</u> hydraulic experimental system is used to provide measured values of the desired pressure

and flow waveforms. The use of such a system allows for greater control of the experimental data than would be possible in an *in vivo* setting and permits direct measurement of the desired parameters. Third, the performance index is determined as the sum of squared error between measured and computed pressure and/or flow for one "cardiac" cycle. Finally, the Gauss-Newton method is applied to minimize the difference between measured and predicted values. The procedure is then used to provide estimates of vessel compliance, peripheral resistance, and severity and location of a stenosis which may be present in the arterial segment of interest.

CHAPTER 2

LITERATURE REVIEW

Many mathematical models of the cardiovascular system have been developed and widely used in the analysis of the physical phenomena associated with circulatory hemodynamics. These models exhibit varying degrees of success in predicting actual physiological behavior. They have been used mainly to help explain how various vessel and fluid parameters affect the shape of pressure and velocity or flow pulses.

However, full use of these models should include the development of techniques for determining system parameters from measured data. This aspect of modeling can provide greater insight into the physical aspects of the circulation and is a means by which the validity of modeling assumptions can be made. Moreoever, if pathological aspects of arterial properties can be faithfully represented by a model, parameter estimation techniques will be a tool for the clinical evaluation of arterial disease. This chapter will present details of past research in these areas.

Mathematical Models

The synthesis of a complete circulatory model is hampered by several factors. First of all, blood is a suspension of particulate matter--cells, etc.--in plasma and as such has a viscosity which depends on the shear rate (McDonald, 1974). Second, the properties of the arterial wall include viscoelastic effects (Noordergraaf, 1978). In addition, cardiovascular geometry is quite irregular. Furthermore,

these properties cannot be directly measured *in vivo*. Consequently, any workable mathematical model of the circulation will require considerable simplification of the physical system.

A major component of the cardiovascular system to be modeled is a segment of artery, free of branches and obstructions. Provided that attention is focused upon arterial sections of moderate size, excluding the capillary beds, for example, blood may be considered to be an incompressible Newtonian fluid (McDonald, 1974). Consequently, the basic equations which describe the pulsatile motion of blood are the Navier-Stokes and continuity equations. Typically, these are expressed in terms of axisymmetric cylindrical coordinates under the assumption of a cylindrical arterial lumen (Noordergraaf, 1978).

An additional set of equations to relate the deformation of the arterial wall to the fluid motion is required. For example, the Navier equations (Noordergraaf, 1978) can be used if the vessel wall is assumed to be elastic, homogeneous and isotropic, but the true nature of an arterial segment is viscoelastic (Noordergraaf, 1978; Westerhof and Noordergraaf, 1970). Unfortunately, determination of the elastic properties of the arterial wall is conducted *in vitro* and thus provides a distorted view of *in vivo* conditions.

Due to the complexity of the full Navier-Stokes equations and the difficulty in obtaining solutions, useful models of blood flow in an arterial segment are typically one-dimensional simplifications. The equations of continuity and axial momentum thus can be expressed as

$$\frac{\partial Q}{\partial x} + \frac{\partial A}{\partial t} = 0 \tag{2.1}$$

$$\frac{\partial Q}{\partial t} + \frac{\partial}{\partial x}(\lambda Q^2/A) = -\frac{A}{\rho}\frac{\partial p}{\partial x} + \frac{\tau_o \pi D}{\rho}. \tag{2.2}$$

In the preceding equations, Q and p are the flow and pressure at axial location x and time t, respectively; A and D are the lumen area and diameter; τ_o is the wall shearing stress; ρ is the blood density; and λ is the ratio of mean squared velocity to mean velocity squared. This form of the governing equations has been used successfully by several researchers (Streeter et al., 1963; Olsen and Shapiro, 1967; Anliker et al., 1971a, 1971b; Schaaf and Abbrecht, 1972; Wemple and Mockros, 1972; Raines et al., 1974; Rumberger and Nerem, 1977). Implementation of Equations 2.1 and 2.2 requires further modeling assumptions in order to relate lumen area A to transmural pressure p, to model the wall shear τ_o, and to represent the momentum correction factor λ.

The most critical of these assumptions concerns the modeling of the area-pressure relationship which characterizes the distensible nature of an artery. The simplest idealization is obtained for an untapered tube in which area and pressure are linearly related by

$$A(p,x) = A_o + C(p(x,t) - p_o) \tag{2.3}$$

where $C = \partial A/\partial p$ is the tube compliance per unit length and A_o is the area at the pressure p_o. This approach has been taken by many researchers (Noordergraaf et al., 1964; Taylor, 1965; Snyder and Rideout, 1968; Westerhof et al., 1969; Welkowitz, 1977). An additional assumption commonly used is that the deviations from the nominal lumen area A_o are small. That is,

$$C|p - p_o|/A_o \ll 1. \tag{2.4}$$

An equation of state based upon analysis of thin-walled pressure vessels (Streeter et al., 1963; Schaaf and Abbrecht, 1972; Wemple and Mockros, 1972) takes the form

$$A(p,x) = A(p_o,x)/(1 - \frac{pD}{hE}) \tag{2.5}$$

and assumes elastic wall behavior. In this equation, E is the vessel modulus of elasticity and h is the wall thickness. Other representations have made use of empirically determined equations. Rooz (1980) fitted a nonlinear relationship

$$A(p,x) = A_o + C_1(p(x,t) - p_o) + C_2(p(x,t) - p_o)^2 \tag{2.6}$$

to data obtained from flexible tube studies.

Raines et al. (1974) assumed a form

$$A(p,x) = A(p_o,x) + \beta \ell n(p/p_o) \tag{2.7}$$

where β is determined experimentally and the area $A(p_o,x)$ at nominal pressure is tapered according to an exponential relationship. Several researchers (Rumberger and Nerem, 1977; Anliker et al., 1978) proposed a state equation

$$A(p,x) = A(p_o,x)\exp(\frac{p - p_o}{\rho c(p,x)c(p_o,x)}) \tag{2.8}$$

where the wavespeed c is modeled from experimental data. Vander Werff (1974) assumed a state equation of the form

$$A(p,x) = A(p_o,x)(1 + \tanh(\frac{p - p_o}{\rho c_o^2})). \tag{2.9}$$

In each of the preceding state equations, area variation depends only on pressure, so that wall viscoelasticity is precluded.

Models which include viscoelastic effects have been uncommon due to a lack of reliable data. However, simple viscoelastic models have been reported (Westerhof and Noordergraaf, 1970; Noordergraaf, 1978). In addition, a model using a complex-valued creep function has been used (Holenstein and Niederer, 1980) although its validity is yet to be verified.

Further modeling assumptions associated with Equation 2.2 concern the form of the friction and convection terms. The wall shear in a one-dimensional situation is not determined by the flow profile and an approximate expression is required. The simplest assumption is that the wall shear stress can be approximated by steady flow conditions in a rigid tube (Poiseuille flow) so that (Raines et al., 1974)

$$\tau_o = -\frac{8\mu Q}{AD}. \tag{2.10}$$

A model which includes unsteady effects is of the form

$$\tau_o = -\frac{8\mu Q}{AD} + \frac{\rho D(\lambda - 1)}{4A}\frac{\partial Q}{\partial t} \tag{2.11}$$

which is derived from considerations of oscillatory flow in an infinite rigid tube (Schaaf and Abbrecht, 1972).

In the latter study, the momentum correction factor was varied from $\lambda = 4/3$ (parabolic profile) to $\lambda = 1$ (flat profile) to assess the effects of the dynamic friction. No appreciable variation was observed. In fact, setting $\mu = 0$ (inviscid) and $\lambda = 1$, so that wall friction

was eliminated, did not produce significant effects. It can be concluded that the form of the friction term is not critical so that Equation 2.10 is a reasonable model.

The momentum correction factor λ was varied (Schaaf and Abbrecht, 1972) to ascertain its significance. The resulting changes in flow and pressure waveforms were not significant. Furthermore, magnitude comparisons showed that the convective term in Equation 2.2 was small compared to the inertia and pressure gradient, so that the omission of convection entirely is a reasonable simplification.

If convection is neglected and the assumptions represented by Equations 2.3, 2.4 and 2.10 are implemented, then Equations 2.1 and 2.2 can be linearized to take the form

$$\frac{\partial Q}{\partial x} + C \frac{\partial p}{\partial t} = 0 \tag{2.12}$$

$$\frac{\partial p}{\partial x} + RQ + L \frac{\partial Q}{\partial t} = 0 \tag{2.13}$$

where $R = 8\pi\mu/A_o^2$ and $L = \rho/A_o$ are the fluid resistance and inertance, respectively. This set of equations has been found to produce satisfactory waveforms (Snyder and Rideout, 1968; Westerhof et al., 1969). Similarity of these equations to the "telegraph equations" of transmission line theory has prompted development of electrical analog models of circulation (Noordergraaf et al., 1964; Taylor, 1965; Welkowitz, 1977).

Results from the linear model have not been as good as those from the nonlinear models for several reasons. First, the assumption of small variations in the lumen area is not valid throughout the arterial system. For example, in the human ascending aorta, area changes on the

order of 12 percent have been reported (Patel et al., 1964) which are not "small" variations. However, changes of around 2 percent are found in the human femoral artery (Patel et al., 1964) so that the linearizing assumption is reasonable in the peripheral circulation. Second, comparisons between waveforms obtained from the linear and nonlinear models indicate that the linear response is considerably noisier than its nonlinear counterpart due to damping which results from nonlinear terms (Schaaf and Abbrecht, 1972; Rooz, 1980).

A characteristic feature of the arterial system is the occurrence of numerous branches. Therefore, the synthesis of a mathematical model of the circulation must include branching effects. Although various attempts have been made to incorporate branches into one-dimensional arterial models, a completely satisfactory model has not been reported. This is because branching flows, even under steady conditions, are inherently not one-dimensional. In fact, helical secondary flows, boundary layer separation and turbulence have been observed (Attinger, 1964; Crowe and Krovetz, 1972; Brech and Bellhouse, 1973; McDonald, 1974). Therefore, severe simplifying assumptions must be made in order to incorporate branches into a model.

The simplest realistic method of modeling a branch involves imposing pressure and flow relationships which are based on steady flow through rigid pipes. In this case, distensibility of the junction is ignored and local transient effects are neglected. This results in the modeling assumptions that the instantaneous pressure in the daughter branches is the same as that at the entrance and that the entering flow rate is the sum of the outflows, i.e.,

$$p_1 = p_2 = p_3 \tag{2.14}$$

$$Q_1 = Q_2 + Q_3 . \tag{2.15}$$

The subscript 1 refers to the entrance to the branch and subscripts 2 and 3 refer to the branch exits.

This approach has been successfully implemented by several researchers (Skalak, 1972; Raines et al., 1974). It is analogous to the voltage and current relationships encountered at a junction in an electrical circuit and thus is basic to electrical analog models (Snyder and Rideout, 1968; Westerhof et al., 1969). Since the dynamic pressure in the circulation is small compared to the unsteady driving pressures (Raines et al., 1974), these assumptions are considered to be satisfactory.

A second method incorporates a flexible branch by imposing the continuity and unsteady Bernoulli equations in the form

$$Q_1 = Q_2 + Q_3 + \frac{dV}{dt} \tag{2.16}$$

$$p_1 - p_i = \frac{\rho}{2} (v_i^2 - v_1^2) + \rho \int_{x_1}^{x_i} (\frac{\partial v}{\partial t}) dx , \quad i = 2,3. \tag{2.17}$$

(Anliker et al., 1978; Holenstein and Niederer, 1980). Subscripts in these equations carry the same meaning as those in Equations 2.14 and 2.15. In addition, V is the volume of the branch and v is the average velocity over the cross section. Although this approach does include dynamic pressure effects, it is based upon the assumption of inviscid fluid and so is probably not a significant improvement over the assumptions stated previously (Raines et al., 1974).

Other approaches to incorporating branching effects do not have a direct physical basis. An example is the assumption that a constant outflow which is independent of local pressure is maintained in bifurcations emanating from a main arterial segment (Wemple and Mockros, 1972). Another example involves replacing discrete branch sites by a distributed seepage term ψ (exit flow per unit length) in the continuity equation, so that

$$\frac{\partial Q}{\partial x} + \frac{\partial A}{\partial t} + \psi = 0 \qquad (2.18)$$

(Skalak and Stathis, 1966).

An area of particular interest to researchers in cardiovascular fluid dynamics is the effect of arterial disease upon the pressure or flow waveforms. Model studies in this area are useful both to gain insight into the causes and mechanics of pathological conditions and to provide means for identifying these conditions. One form of arterial disease which is of special importance is the occurrence of arterial stenoses, which are localized constrictions usually caused by the deposition of atherosclerotic plaque.

The specific disorders which bring about the formation of a stenotic obstruction are not well-understood. However, there are specific effects on the pressure and flow waveforms that result from such constrictions. In particular, a stenosis is found to cause a drop in pressure and usually a reduced flow rate, although variation in the resistance in the vascular bed can act to maintain an adequate mean flow (Young et al., 1975; Young, 1979). Experimental evidence also indicates that there is little change in the mean flow until the lumen

area has been critically reduced. This "critical stenosis" is generally accepted to refer to a reduction in area of approximately 80 percent (Young, 1979).

Modeling considerations for a localized stenosis are based upon several factors. First, due to the buildup of plaque, a stenosis is significantly stiffer than the surrounding arterial wall, so that the assumption of a rigid constriction is reasonable. Second, for a localized stenosis, the change in geometry is quite abrupt compared to the gradual taper of a healthy arterial segment, so that modeling a stenosis as a blunt hollow plug is justified (Young, 1979). In addition, eccentricity of the stenosis lumen has been found to have little effect in the case of a severe stenosis (Seeley and Young, 1976) so that an axisymmetric geometry is acceptable.

Due to the assumption of a rigid constriction, the instantaneous flow waveforms at the proximal (nearest the heart) and distal ends of the stenosis must be identical. However, there will be a drop in pressure due to losses caused by turbulence, inertial effects, etc. Thus, a suitable mathematical model of a stenosis will represent this drop in pressure. One such model is expressed as

$$\Delta p = \frac{4K_v\mu}{\pi D_o^3} Q + \frac{8K_t\rho}{\pi^2 D_o^4}\left(\frac{A_o}{A_1} - 1\right)^2 |Q|Q + \frac{4K_u\rho L_s}{\pi D_o^2}\frac{dQ}{dt} \qquad (2.19)$$

(Young, 1979), where K_v, K_t and K_u are empirical constants; D_o and A_o are the diameter and area of the unobstructed tube; and L_s and A_1 are the stenosis length and lumen area. The three terms in Equation 2.19 represent viscous losses, turbulent losses associated with the sudden

expansion distal to the stenosis, and losses due to the inertial effects of fluid acceleration past the constriction, respectively.

The empirical coefficients K_v, K_t and K_u will depend upon the stenosis geometry and upon the frequency parameter $\alpha = D_o\sqrt{\rho\omega/\mu}/2$, where ω is the natural (circular) frequency of the pulsatile flow. Experimental evidence obtained in _in vitro_ models indicates that K_t is adequately approximated by a value of 1.52 for blunt axisymmetric constrictions (Seeley and Young, 1976). The coefficient K_u may be represented by a value of 1.2 for the blunt axisymmetric constriction (Young and Tsai, 1973). In addition, for the range of frequency parameter commonly encountered in physiological settings, local inertial effects are relatively small, so that K_v can be reasonably approximated by the expression

$$K_v = 32 \left(\frac{L_a}{D_o}\right)\left(\frac{A_o}{A_1}\right)^2 \tag{2.20}$$

with

$$L_a = 0.83\, L_s + 1.64\, D_1 \tag{2.21}$$

where D_1 is the stenosis lumen diameter (Seeley and Young, 1976). Extensive _in vivo_ testing indicates that Equation 2.19 provides good agreement with experimental data (Young et al., 1975).

A similar model has been proposed of the form

$$\Delta p = \frac{\rho}{2}(v_2^2 - v_1^2) + \rho \int_{x_1}^{x_2} \left(\frac{\partial v}{\partial t}\right) dx + \frac{\rho}{2} v_1^2 \left(\frac{A_o}{A_1} - 1\right)^2 + \frac{8\pi\mu L_s}{A_1}\left(\frac{A_o}{A_1}\right) v_1 \tag{2.22}$$

(Anliker et al., 1978). In addition, models have been formulated by Clark (1976a, b) and Newman et al. (1979) which are applicable to aortic stenoses.

The final requirement necessary to formulate a mathematical model of a section of the arterial tree is the specification of boundary conditions. At the ends of a section, either a flow or a pressure waveform can be imposed. At the distal end, though, a more realistic boundary condition is terminal impedance. Typically this can be expressed as a pure resistance so that distal pressure p and flow Q are related by

$$p = Z\,Q \tag{2.23}$$

where Z is the constant resistance. However, due to vessel distensibility in the peripheral beds, the ratio of pressure to flow should include compliance variation such as

$$Z = R_1 + \frac{R_2\,(1 - jR_2C_T\omega)}{1 + R_2^{\,2}C_T^{\,2}\omega^2} \tag{2.24}$$

where $j = \sqrt{-1}$, R_1 and R_2 are pure resistances and C_T is a lumped peripheral compliance. This allows for differences in phase of the pressure and flow waveforms (Raines et al., 1974).

Due to both the complexity and the nonlinear nature of the governing model equations, numerical solution techniques are required to produce pressure and flow waveforms from a mathematical model. For analog models, this is accomplished directly by analog computation techniques (Snyder and Rideout, 1968; Westerhof et al., 1969). Other techniques include the method of characteristics (Streeter et al., 1963;

Olsen and Shapiro, 1967; Wemple and Mockros, 1972; Vander Werff, 1974; Anliker et al., 1978), perturbation methods (Olsen and Shapiro, 1967), and finite difference techniques (Raines et al., 1974).

It is interesting that the finite element method (Desai and Abel, 1972; Zienkiewicz, 1977) has not found more use in the analyis of the models described above. Some work has been reported for two-dimensional models (Kandarpa and Davids, 1976). Recently, however, use of the finite element method with one-dimensional models has been made by Rooz (1980) and Young et al. (1980). The advantage of this technique is that it easily supports variation in system properties and can handle nonlinear equations with relative ease.

Parameter Estimation

The main use of models in cardiovascular research has been to gain insight into the physical aspects of the circulatory system. That is, once the model has been shown to provide satisfactory agreement with a physical system, model parameters can be adjusted and the variations in model response investigated. Another model application that offers the possibility of clinical use is the parameter estimation technique.

In these methods, model input is obtained from physical data and the model response is compared to other data. The difference between model and experimental data is compared and the model is systematically varied by adjusting system parameters until the difference is minimized. If the model satisfactorily simulates the physical system, the resulting parameters will characterize the phenomena of interest. Many such

estimation techniques are available and descriptions can be found in the references by Bard (1974) and Beck and Arnold (1977).

Although parameter estimation techniques have found widespread use in many areas of science and engineering, acceptance of these methods by researchers in the biomedical disciplines has not been great. However, surveys of physiological applications can be found in the literature (Beneken, 1972; Rideout and Beneken, 1975; Bekey and Yamashiro, 1976). These reports indicate various estimation techniques and results, and also give insight to some of the reasons why these techniques have not been more widely used. One of these problems is the difficulty in obtaining accurate experimental data which are required both for model input and for validation of the estimated parameters.

Technical problems such as model sensitivity to parameters, lack of uniqueness of the estimated values and computation costs are also reported. In addition, there is a distrust by medical researchers of values obtained indirectly (Bekey and Yamashiro, 1976). More research of applications of estimation techniques is necessary to solve these problems, but the reported results are promising.

Wesseling et al. (1973) reported estimation results using a four compartment lumped parameter model of the arterial system from the axilla to the wrist. The parameters of interest consisted of segment resistance, compliance, and inertance and branch resistance. They were expressed in terms of lumen area, modulus of elasticity of the vessel wall and branch conductance so that 12 parameters were involved. The

model input consisted of the uncalibrated axilla pressure pulse and the output wrist waveform was compared to the measured pulse. Since the model consisted of an analog circuit, parameter variation was performed manually. The resulting estimated values were within the physiological range.

Sims (1972) used a ten compartment lumped parameter model with three peripheral resistances. Measured data consisted of three pressure and two flow waveforms obtained from canine experiments. The parameters of interest included the ten compartmental compliances and the three peripheral resistances which were estimated using Marquardt's method. Although the technique converged in a small number of iterations, some of the estimated parameters showed considerable error, even when model input was generated by the model itself.

Dennison et al. (1972) implemented a lumped parameter model by solving the resulting differential equations on a digital computer. The model was used to produce pressure waveforms assuming nominal values of two compliances plus an inertance and resistance. These parameters were estimated using a generalized Newton-Raphson or quasilinearization technique and good agreement was typically observed within five iterations. In addition, it was observed that errors of 15 percent in the known parameters could produce an order of magnitude variation in the estimated values.

A lumped parameter model programmed into an analog computer was used by Chang et al. (1974) to estimate nine parameters including vessel radii, elasticity, lengths and resistances. Model input was a

pressure waveform with two pressures and two flows being used to measure the absolute value error. The Hooke and Jeeves pattern search technique was used to minimize the performance index. Although estimated parameters were within 5 percent for model-to-model comparisons, it was found that 50 to 75 iterations were required for convergence.

A transfer function representation of a lumped parameter model has been used (Welkowitz et al., 1972; Strano, 1973; Welkowitz, 1977) to determine 9 parameters characteristic of the aorta. These included taper coefficient, entrance area, hoop elasticity and equivalent blood viscosity. The model input consisted of the ratio of proximal to distal pressure, heart frequency and distance between measuring sites. The performance index was computed as a weighted residual "cost function" which included both magnitude and phase errors. A hybrid technique consisting of model reference, elementary learning, figure of merit, and modified gradient methods was used to minimize the cost function, and the results agree favorably with published values.

Clark et al. (1980) employed a two-stage parameter estimation scheme consisting of the Prony method for initial parameter values followed by Marquardt's method to obtain final results. The mathematical model was a two compartment lumped parameter system and the parameters to be identified were two compliances, a resistance, an inertance and the initial flow. The left ventricular pressure was used as model input and pressures in the ascending aorta and proximal brachial artery were used for comparison purposes. Model-to-model comparisons showed

good agreement in estimated parameters and results from human subject data were physically realistic.

Bourne and Kitney (1978) modeled an arterial section by a lumped parameter model in order to estimate overall arterial compliance and total peripheral resistance. A single pressure waveform was used to determine the performance index which was minimized by the Rosenbrock method, a gradient technique, and good model-to-model agreement was produced. In addition, random noise was superimposed upon the pressure waveform. The estimated compliance value was affected by the noise while the peripheral resistance was relatively insensitive.

Young et al. (1980) used a finite element simulation of the linearized arterial model, Equations 2.12 and 2.13 and the Gauss-Newton minimization procedure to estimate arterial compliance and radius and peripheral resistance. Model input consisted of proximal pressure or flow waveforms and distal pressure, flow or resistance. Proximal or distal flow or pressure waveforms were used to determine the sum of squared error. Vessel compliance and, when applicable, peripheral resistance could be accurately estimated for some but not all combinations of model inputs and observed waveforms. However, the vessel radius could not be accurately estimated due to lack of model sensitivity. Comparisons between estimated parameters and those obtained from a hydraulic <u>in vitro</u> model showed good agreement.

The use of parameter estimation techniques in the evaluation of arterial disease has suffered a noticeable lack of attention in the literature. However, one notice of results (Greene et al., 1980)

reports the use of noninvasive flow measurements in conjunction with a statistical pattern recognition technique to assess carotid arterial disease. Quantitative stenosis parameters were not obtained, but rather the technique was used to classify human subjects as normal or suffering from a slight or severe obstruction. From a pool of 57 subjects, a 100 percent success rate of screening was obtained with subsequent angiographic confirmation of disease.

The literature presented in this review indicates that considerable research has been performed in the areas of mathematical modeling and parameter estimation associated with cardiovascular fluid dynamics. However, the finite element method has not been widely used despite its versatility. In addition, parameter estimation techniques have not been applied to the determination of quantitative characteristics of occlusive arterial disease. This dissertation will provide preliminary results to help bridge that gap.

CHAPTER 3

MATHEMATICAL MODEL

The mathematical model which was used to simulate an arterial segment for the present study consists of the governing equations which describe pulsatile pressure and flow through a straight flexible tube segment, a branch and a stenosis, and the numerical approximation used to solve these equations. The straight tube equations are two coupled linear partial differential equations. The stenosis is modeled by an empirical formula which is representative of the geometry of the constriction and a simplified branch is assumed. The set of governing equations is approximated and solved using the finite element method. Development of the model equations and finite element scheme will be presented here with additional details provided in Appendix A.

Straight Tube Model

The governing equations for incompressible pulsatile flow and pressure in a straight segment of flexible tube describe conservation of mass and momentum, respectively,

$$\frac{\partial Q}{\partial x} + \frac{\partial A}{\partial t} = 0 \tag{3.1}$$

$$\frac{\partial Q}{\partial t} + \frac{\partial}{\partial x}(\lambda Q^2/A) = -\frac{A}{\rho}\frac{\partial p}{\partial x} + \frac{\tau_o \pi D}{\rho} . \tag{3.2}$$

Axial motion of the tube has been neglected in these equations. In addition, a constitutive relationship for determining area variation is required,

$$A = A(p,x) \tag{3.3}$$

which allows for area change as a function of both pressure and axial

location. In this form, viscoelastic effects are not considered. In the convective term of Equation 3.2, the coefficient λ depends on the nature of the velocity profile. For example, $\lambda = 1$ for a flat profile while $\lambda = 4/3$ for a steady laminar (parabolic) profile.

Several assumptions and simplifications are made to reduce Equations 3.1 through 3.3 to the working model. The area-pressure relationship is assumed to be linear, so that

$$A(p,x) = A_o + C(p(x,t) - p_o) \tag{3.4}$$

and that area fluctuations are small, i.e.,

$$C|p(x,t) - p_o|/A_o << 1. \tag{3.5}$$

The coefficient C is commonly referred to as the vessel compliance. It is further assumed that the tube is not tapered and is homogeneous so that A_o and C are constants. A quadratic equation of state has been shown to provide better agreement with measured data, but the linear model chosen here yields satisfactory results (Rooz, 1980).

Due to the one-dimensional nature of Equations 3.1 and 3.2, the wall shear stress τ_o is not determined by the flow profile. Since friction is not expected to be a major factor in the flow, the assumption of steady laminar (Poiseuille) friction is made, so that

$$\tau_o = -\frac{8\mu Q}{AD}. \tag{3.6}$$

Since convection effects are expected to be small the convective acceleration term in Equation 3.2 is neglected. Finally, since variations in cross-sectional area are assumed to be small, the nominal area A_o is used instead of the instantaneous area A(p,x). This yields the linearized

one-dimensional equations

$$\frac{\partial Q}{\partial x} + C\frac{\partial p}{\partial t} = 0 \tag{3.7}$$

$$\frac{\partial p}{\partial x} + RQ + L\frac{\partial Q}{\partial t} = 0 , \tag{3.8}$$

where $R = 8\pi\mu/A_o^2$ and $L = \rho/A_o$. Tube geometry is shown in Figure 3.1a.

Branch Model

The mathematical model for a branch consists of the equations

$$P_1 = P_2 = P_3 \tag{3.9}$$

$$Q_1 = Q_2 + Q_3 \tag{3.10}$$

which are commonly used in the analysis of steady flow through piping networks. Figure 3.1b illustrates the branching geometry and the subscripts in Equations 3.9 and 3.10. These equations neglect such effects as distensibility, friction, turbulence and development of secondary flows but will be used as a first approximation. Additional research into the nature of branching effects was beyond the scope of this dissertation and will not be considered.

Stenosis Model

The governing equations for a stenosis are based upon research by Young et al. (1975). For the stenosis geometry depicted in Figure 3.1c the flow relationship is simply

$$Q_1 = Q_2 \equiv Q \tag{3.11}$$

which assumes a rigid constriction. The pressure drop across the stenosis can be expressed as

Figure 3.1a. Schematic diagram of straight tube segment
Figure 3.1b. Schematic diagram of branch
Figure 3.1c. Schematic diagram of stenosis

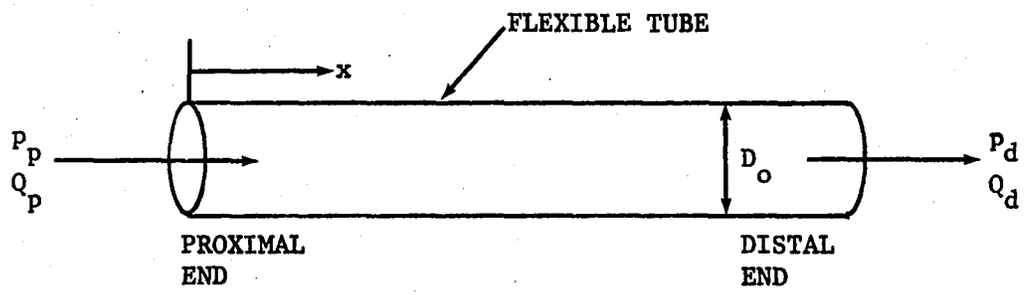
FLEXIBLE TUBE
x
P_p
Q_p
D_o
P_d
Q_d
PROXIMAL END
DISTAL END

a

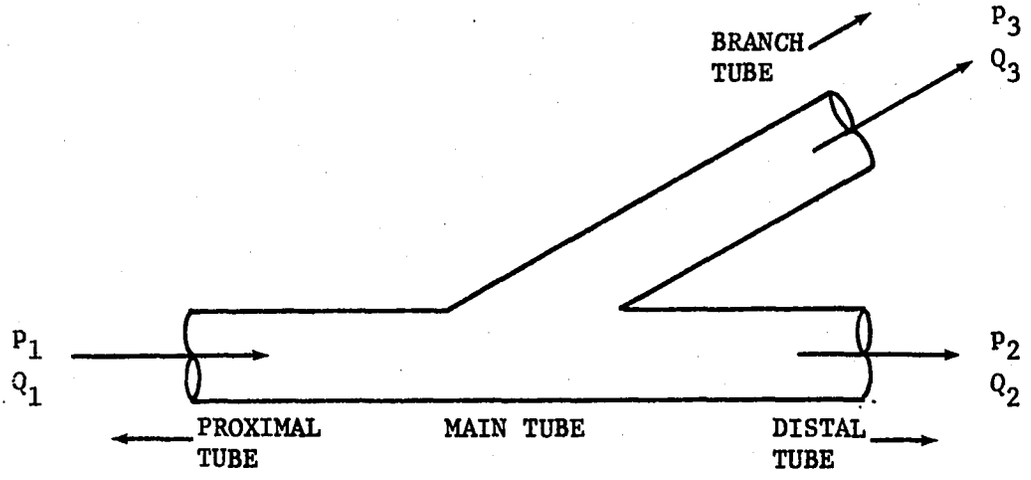
BRANCH TUBE
P_3
Q_3
P_1
Q_1
P_2
Q_2
PROXIMAL TUBE
MAIN TUBE
DISTAL TUBE

b

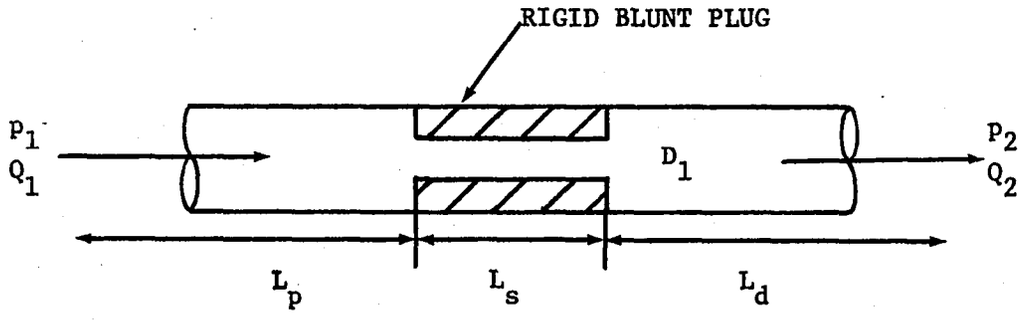
RIGID BLUNT PLUG
P_1
Q_1
D_1
P_2
Q_2
L_p
L_s
L_d

c

$$p_1 - p_2 = \frac{4K_v\mu}{\pi D_o^3} Q + \frac{8K_t\rho}{\pi^2 D_o^4}\left(\frac{A_o}{A_1} - 1\right)^2 |Q|Q + \frac{4K_u\rho L_s}{\pi D_o^2}\frac{dQ}{dt} . \quad (3.12)$$

The first term represents viscous losses, the second characterizes losses due to the sudden expansion and contraction, and the third includes losses due to the acceleration of the fluid through the constriction. The empirical coefficients K_t and K_u depend upon stenosis geometry and upon the frequency parameter $\alpha = D_o\sqrt{\rho\omega/\mu}/2$, but may be approximated by 1.52 and 1.2, respectively, for simple stenosis geometries. The constant K_v is determined as $32(L_a/D_1)(A_o/A_1)^2$ where $L_a = 0.83L_s + 1.83D_1$.

Boundary Conditions

Solution of the governing equations to produce particular waveforms requires that boundary and initial conditions be imposed. The straight tube Equations 3.7 and 3.8 require two boundary conditions which could be either a flow or a pressure waveform specified at the proximal and distal ends of the tube. In addition, a terminal resistance $Z = p/Q$ can be prescribed at the distal end. In some cases, Z can be assumed to be a constant or pure resistance.

The full mathematical model is constructed as several straight tube segments which are connected by a branch and/or a stenosis. Therefore, the boundary conditions applied at these connections are Equations 3.9 and 3.10 for a branch and Equations 3.11 and 3.12 for a stenosis.

The initial axial distribution of flow and pressure in the system is not known, in general, so correct starting values can not be assigned. Due to damping in the model, however, transient fluctuations caused by improper initial conditions will decay so initial values are not critical.

Numerical Solution

In the absence of a stenosis, the pressure and flow waveforms in a straight flexible tube can be determined analytically, since the governing equations are linear. However, if a stenosis is present, the system of equations is nonlinear because of the pressure drop given by Equation 3.12. An analytical solution is then precluded and a numerical integration scheme must be employed to solve the mathematical model.

A versatile technique which has found use in biomechanics but little exposure in biofluids research is the finite element method. The finite element method allows differential equations to be approximated by systems of algebraic equations and is thus well-suited to digital computer applications. In this study, the axial variation in pressure and flow is approximated by finite element equations and the resulting system of ordinary differential equations in time is solved by numerical integration. Although temporal as well as spatial dependence can be approximated using the finite element method (Rooz, 1980), this approach is not pursued here.

As described in Appendix A, a linear approximation $Q^e(x,t)$ to the actual instantaneous flow distribution $Q(x,t)$ in an arterial section or element can be expressed as

$$Q^e(x,t) = N_i(x)Q(x_i,t) + N_j(x)Q(x_j,t), \quad x_i \leq x \leq x_j \tag{3.13}$$

where x_i and x_j are the axial coordinates of the element endpoints or nodes and

$$N_i(x) = \frac{x_j - x}{x_j - x_i}, \quad N_j(x) = \frac{x - x_i}{x_j - x_i} \tag{3.14}$$

are linear interpolating polynomials or shape functions. The smaller the element length $L^e = x_j - x_i$, the better the accuracy of the element approximation. In this manner, the flow and pressure can be approximated in piecewise linear fashion over the entire tube length. It remains to fit this interpolation scheme to the mathematical model.

The element functions $Q^e(x,t)$ and $p^e(x,t)$ will not, in general, be solutions to the governing equations for an element. For example, inserting $Q^e(x,t)$ and $p^e(x,t)$ into Equation 3.7 yields

$$\frac{\partial Q^e}{\partial x} + C \frac{\partial p^e}{\partial t} = r \neq 0 . \tag{3.15}$$

For best approximation, the residual r in Equation 3.15 must be minimized in some fashion.

The Galerkin method is a technique which minimizes the residual by forcing it to be "orthogonal" to the shape functions $N_i(x)$ and $N_j(x)$ in the sense that

$$\int_{x_i}^{x_j} N_k(x) \left(\frac{\partial Q^e}{\partial x} + C \frac{\partial p^e}{\partial t}\right) dx = 0 , \quad k = i,j. \tag{3.16}$$

As described in Appendix A, this method applied to the residual in Equation 3.15 yields the element equations

$$\frac{dp_i}{dt} = \frac{1}{CL^e}(Q_i(t) - Q_j(t)) \tag{3.17}$$

$$\frac{dp_j}{dt} = \frac{1}{CL^e}(Q_i(t) - Q_j(t)) \tag{3.18}$$

where $Q_i(t) = Q(x_i,t)$ and $p_i(t) = p(x_i,t)$ are the nodal flow and pressure waveforms at node i. The flow gradient $\partial Q/\partial x$ has simply been replaced by

a difference quotient $\Delta Q/L^e$. This underscores the fact that interpolation accuracy is dependent upon element length.

Similarly, the Galerkin technique applied to Equation 3.8, which is the momentum equation, yields the element equations

$$\frac{dQ_i}{dt} = -\frac{R}{L} Q_i(t) + \frac{1}{LL^e}(p_i(t) - p_j(t)) \tag{3.19}$$

$$\frac{dQ_j}{dt} = -\frac{R}{L} Q_j(t) + \frac{1}{LL^e}(p_i(t) - p_j(t)). \tag{3.20}$$

Thus, Equations 3.17 through 3.20 provide a set of coupled linear first order ordinary differential equations for the flow and pressure at the nodes of an element.

For a long section of tube, many elements must be used in order to guarantee accuracy of the solution. The element equations for adjacent elements are combined by the direct stiffness method. Thus, let i, j and k be node numbers for two consecutive elements. The pressure rate at the common node j can be written for the two elements as

$$\frac{dp_j}{dt} = \frac{1}{CL^e}(Q_i(t) - Q_j(t)) \tag{3.21}$$

and

$$\frac{dp_j}{dt} = \frac{1}{CL^e}(Q_j(t) - Q_k(t)) , \tag{3.22}$$

respectively. It has been assumed that the two elements have identical lengths and material properties. If Equations 3.21 and 3.22 are added and the the result divided by two, the result is the nodal equation for the pressure rate at node j,

$$\frac{dp_j}{dt} = \frac{1}{2CL^e}(Q_i(t) - Q_k(t)). \tag{3.23}$$

A similar analysis using Equations 3.19 and 3.20 yields the nodal equation for flow rate

$$\frac{dQ_j}{dt} = -\frac{R}{L} Q_j(t) + \frac{1}{2LL^e}(p_i(t) - p_j(t)). \tag{3.24}$$

Equations 3.23 and 3.24 are valid at all nodes except the proximal and distal ends of a straight tube segment where Equations 3.17 through 3.20 are still applicable.

The finite element approximation for a straight flexible tube with constant properties and equal element lengths is thus the system of equations

$$\frac{d\underline{\delta}}{dt} = [K]\underline{\delta} \tag{3.25}$$

where

$$\underline{\delta} = \{Q_1, p_1, Q_2, p_2, \ldots, Q_N, p_N\}^T \tag{3.26}$$

is the vector of nodal degrees of freedom and [K] is the matrix of coefficients. In Equation 3.26, N is the number of nodes in the finite element approximation of the tube section and T means transpose.

Boundary conditions may now be inserted into the approximation scheme. For example, if the proximal flow waveform $Q(x_1,t)$ is known, then the first nodal equation for Q_1 is eliminated from Equation 3.25 and all subsequent occurrences of Q_1 are replaced by $Q(x_1,t)$. The procedure for specifying a pressure boundary condition is similar.

If the distal boundary condition is to be specified as a known

peripheral resistance $Z = p/Q$, either the distal nodal pressure or flow may be eliminated from Equation 3.25. For example, if the nodal flow is to be dropped, all occurrences of Q_N are replaced by p_N/Z.

Equations 3.9 and 3.10 which characterize a branch are inserted into the finite element model in the following manner. Let i represent the node number at the branch entrance and let j and k be the node numbers for the exits. Equations 3.9 and 3.10 can thus be written as

$$p_i = p_j = p_k \tag{3.27}$$

$$Q_i = Q_j + Q_k. \tag{3.28}$$

The nodal equations in Equation 3.25 for p_j, p_k and Q_i are eliminated. All subsequent occurrences of p_j or p_k are replaced by p_i and all occurrences of Q_i are replaced by $Q_j + Q_k$.

The stenosis model Equations 3.11 and 3.12 are implemented as follows. Let i and j represent node numbers for the proximal and distal ends of the stenosis, respectively. Equations 3.11 and 3.12 thus appear as

$$Q_i = Q_j = Q \tag{3.29}$$

$$p_i - p_j = aQ + b|Q|Q + c\frac{dQ}{dt} \tag{3.30}$$

where a, b and c represent the coefficients in Equation 3.12. Equation 3.30 can be rearranged as

$$\frac{dQ}{dt} = \frac{1}{c}(p_i - p_j - aQ - b|Q|Q). \tag{3.31}$$

Therefore, the nodal equation for Q in Equation 3.25 can be eliminated and the nodal equation for Q_i replaced by Equation 3.31. In addition, all remaining occurrences of Q_j in Equation 3.25 are replaced by Q_i.

The mathematical model has now achieved its final form

$$\frac{d\underset{\sim}{\delta}}{dt} = \underset{\sim}{[K]}\underset{\sim}{\delta} \; . \tag{3.32}$$

The coefficient matrix $\underset{\sim}{[K]}$ will be constant for either a straight or branched tube system in the absence of a stenosis, but will be flow-dependent otherwise due to the form of the stenosis model Equation 3.31.

An algorithm for solving Equation 3.32 must therefore be applicable to nonlinear systems. The method chosen for this study was a Runge-Kutta type variable step size numerical integration procedure (Christiansen, 1970) which is available as the subroutine DASCRU in the International Mathematical and Statistical Libraries' subroutine package (Simon, 1975).

CHAPTER 4

EXPERIMENTAL MODEL

A relatively simple *in vitro* model was devised to satisfy several needs. In order to validate the mathematical model described in Chapter 3, data were required for use as boundary conditions for the governing equations and for determining the coefficients in those equations. The parameter estimation scheme, to be presented in Chapter 5, requires additional data to compute a performance index and to provide values for comparison with the estimated parameters. An advantage of using such a physical model is that modifications of the system, such as varying the pulse frequency or including a stenosis, can be readily achieved. Direct measurement of the experimental parameters is also feasible. In addition, it is possible to maintain steady state operation of the system which is often not the case in a physiological subject.

System Design

A schematic diagram of the *in vitro* model is presented in Figure 4.1. The main system component was a flexible tube test section containing a branch and a stenosis. The flow was produced by a pulsatile pump and the clamps downstream from the test section provided peripheral resistances. The pulsatile flow and pressure waveforms were sampled at several locations and the resulting signals were digitized and stored for subsequent analysis and transfer to a digital computer.

The test section consisted of three sections of 6.35 mm-ID latex Penrose drainage tubing 45.7 cm in length. To prevent axial motion of

Figure 4.1. Schematic diagram of *in vitro* experimental apparatus

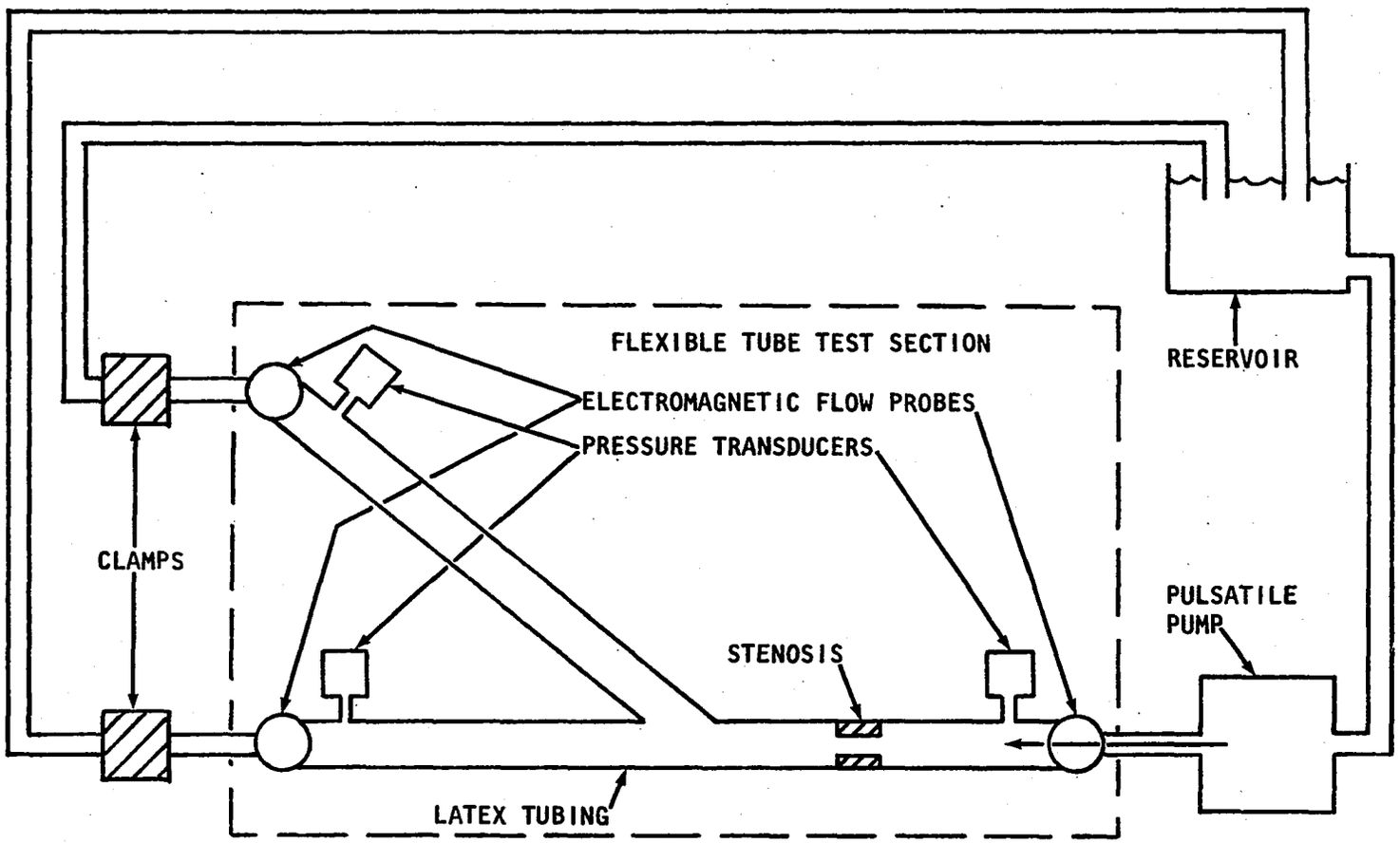
FLEXIBLE TUBE TEST SECTION
RESERVOIR
ELECTROMAGNETIC FLOW PROBES
PRESSURE TRANSDUCERS
CLAMPS
PULSATILE PUMP
STENOSIS
LATEX TUBING

the tubes, they were stretched to a length of 52 cm and the ends were attached either to the branch or to the fittings at the upstream and downstream sections of the test section. The fittings and the branch were fixed to the laboratory bench. The branch consisted of a piece of plexiglass into which was drilled a 6.35 mm-ID bifurcating channel. The stenosis was a blunt cylindrical plug 1.5 cm in length, 6.35 mm in diameter. An axisymmetric lumen, 2.0 mm in diameter was drilled into the plug. The stenosis was force fit into the proximal tubing section and clamped in place.

Pressures were sampled by three strain gage type pressure transducers (Statham P23Db) which were attached to the system via blunt hypodermic needles inserted through the fittings at the ends of the test section. The needles were mounted so that their tips were flush with the inner surface of the tubing to minimize flow disturbances. Flows were measured by three in-line electromagnetic flow probes (In Vivo Metrics) with 3 mm lumen diameters which were located at the ends of the test section. These probes were connected to electromagnetic flow meters (Biotronix BL-610).

The pulsatile flow was produced by an adjustable stroke pump powered by a variable speed motor. Two clamps downstream from the test section were used to maintain sufficient pressure in the system to prevent tubing collapse and to allow variation of flow in the downstream sections. The fluid used was physiological saline with a density of 0.997 gm/cm^3 and a viscosity of 0.0089 $dyne\text{-}sec/cm^2$.

The pressure transducers and flow meters were interfaced with a 12-channel Grass polygraph. The polygraph contained bridge circuits for

the pressure transducers and filters to eliminate high frequency noise. Output from the circuitry was displayed on the polygraph so that visual control of waveforms could be maintained.

Output signals were digitized using a PDP-8/e minicomputer equipped with an A/D converter and built-in clock. A sampling rate of 100/sec was maintained for 2-1/2 seconds for each input channel. The digitized waveforms were subsequently calibrated and stored for transfer to punched paper tape.

Calibration of the pressure channels was made via static measurements. That is, a static pressure was maintained in the system and measured with a manometer attached to the system through a tap in the branch. Flow calibration was effected by timing a measured quantity of fluid under steady flow conditions. The transducer signals were digitized and the calibration factors were determined using the minicomputer.

After calibration was completed, the vessel compliance was determined by direct measurement for each tubing section in turn. For example, to obtain the variation in area of the proximal tube due to changes in pressure, this section was isolated by clamping the distal tubes immediately downstream from the branch and clamping the feed tube upstream from the test section. Fluid was injected in 1.0 cm^3 increments through the tap in the branch and the pressure increase was recorded. The incremental volume was divided by the length of the tube section to produce the change in lumen area relative to the baseline of nominal area at atmospheric pressure. The results of these tests are shown in Figure 4.2. The compliance for each section was determined as the slope, dA/dP, of the

Figure 4.2. Change in cross-sectional area versus change in static pressure for branched tube model

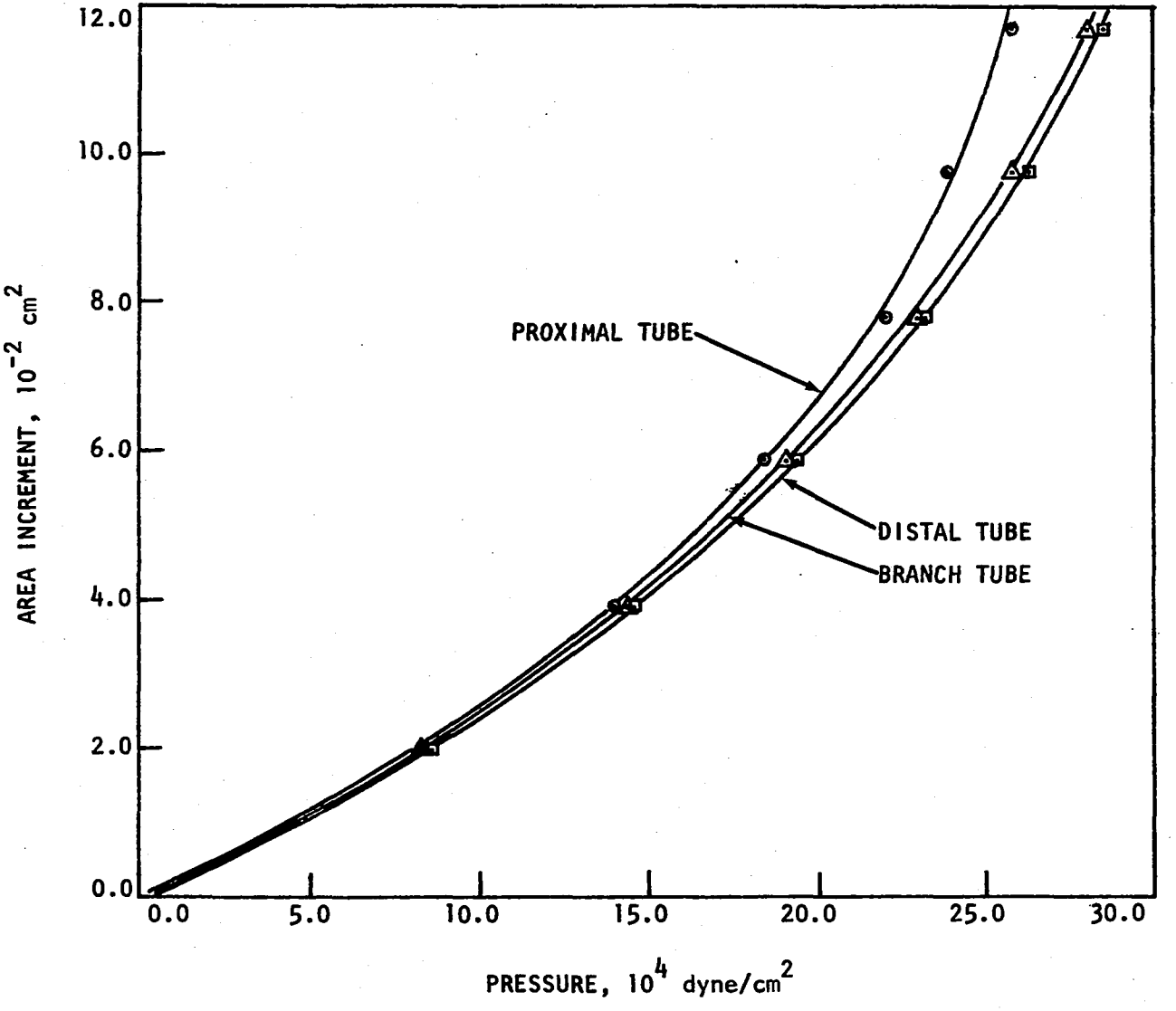
12.0
10.0
8.0
6.0
4.0
2.0
0.0
AREA INCREMENT, 10^{-2} cm^2
PROXIMAL TUBE
DISTAL TUBE
BRANCH TUBE
0.0
5.0
10.0
15.0
20.0
25.0
30.0
PRESSURE, 10^4 dyne/cm^2

corresponding area-pressure curve evaluated at the mean pressure of the pulsatile flow trial.

To obtain the pulsatile pressure and flow waveforms, the pump stroke and distal clamps were adjusted to that the tubing did not collapse during flow. The system was allowed to operate for several minutes in order to flush the test section of air bubbles and to adjust the motor frequency to the desired rate. The test section was then clamped off and pressurized and stopcocks connected to the pressure transducers were opened to allow bubbles to escape from the transducers and to reduce the system pressure and flow to baseline values of atmospheric pressure and zero flow. The baseline values were sampled and recorded. The system was then returned to operation and the polygraph display was monitored to check for steady state conditions. The flows and pressures were sampled, digitized and punched onto paper tape for transfer to a large digital computer (Itel AS/6). The Fourier coefficients of the waveforms were obtained by numerical integration.

Measured Data

For each section, the frequency parameter $\alpha = D_o\sqrt{\omega\rho/\mu}\,/2$ and the Reynolds number $\rho v D_o/\mu$ for both mean and peak flow were computed. The peripheral resistance for each downstream section was calculated as the average of the instantaneous pressure divided by instantaneous flow for one "cardiac" cycle. The nominal diameter, area and compliance were determined at the mean pressure at which pulsatile flow tests were run. A summary of these data is contained in Table 4.1.

Table 4.1. Summary of experimental parameters

Section	Frequency Parameter $D_o\sqrt{\omega\rho/\mu}/2$	Reynolds Number $\rho v D_o/\mu$ Mean	Reynolds Number $\rho v D_o/\mu$ Peak	Area, A_o cm^2	Diameter, D_o cm	Section Length cm	Compliance $cm^4/dyne$	Resistance dyne-s/cm^5
Proximal	8.96	1463	4542	0.34	0.66	52	3.5×10^{-7}	-
Distal	8.74	591	989	0.33	0.65	52	2.9×10^{-7}	20300
Branch	8.74	865	964	0.33	0.65	52	2.9×10^{-7}	14000

Frequency f = 1.04 Hz.

Stenosis length L_s = 1.5 cm.

Stenosis area ratio A_o/A_1 = 10.1.

CHAPTER 5

PARAMETER ESTIMATION TECHNIQUE

As previously discussed, parameter estimation techniques provide a means of extracting unknown parameter values indirectly from observable data. In general, these methods require a mathematical model which simulates the physical system and contains the desired parameters as undetermined coefficients. A means for matching the model response to the observable data by variation of the model parameters is also needed. In this chapter, the Gauss-Newton minimization technique is applied to the error between mathematical model response and experimental data described in the preceding chapters. The derivation of the Gauss-Newton method is outlined in Appendix B.

A schematic diagram of the parameter estimation process is presented in Figure 5.1. First, the mathematical model is solved using input data from the physical system with initial estimates for the unknown parameter values. The resulting model response is compared to the corresponding observed data and the performance index is computed. A minimization algorithm reduces the difference by varying the parameter vector components. If the improved parameter values satisfy some termination criterion, the procedure ceases and the estimated values represent the best fit of the mathematical model to the physical system. If the termination criterion is not met, the improved parameter values are used in place of the initial estimates in the mathematical model and the process is repeated.

In this study, the parameter estimation procedure was used to try to

Figure 5.1. Schematic diagram of parameter estimation procedure

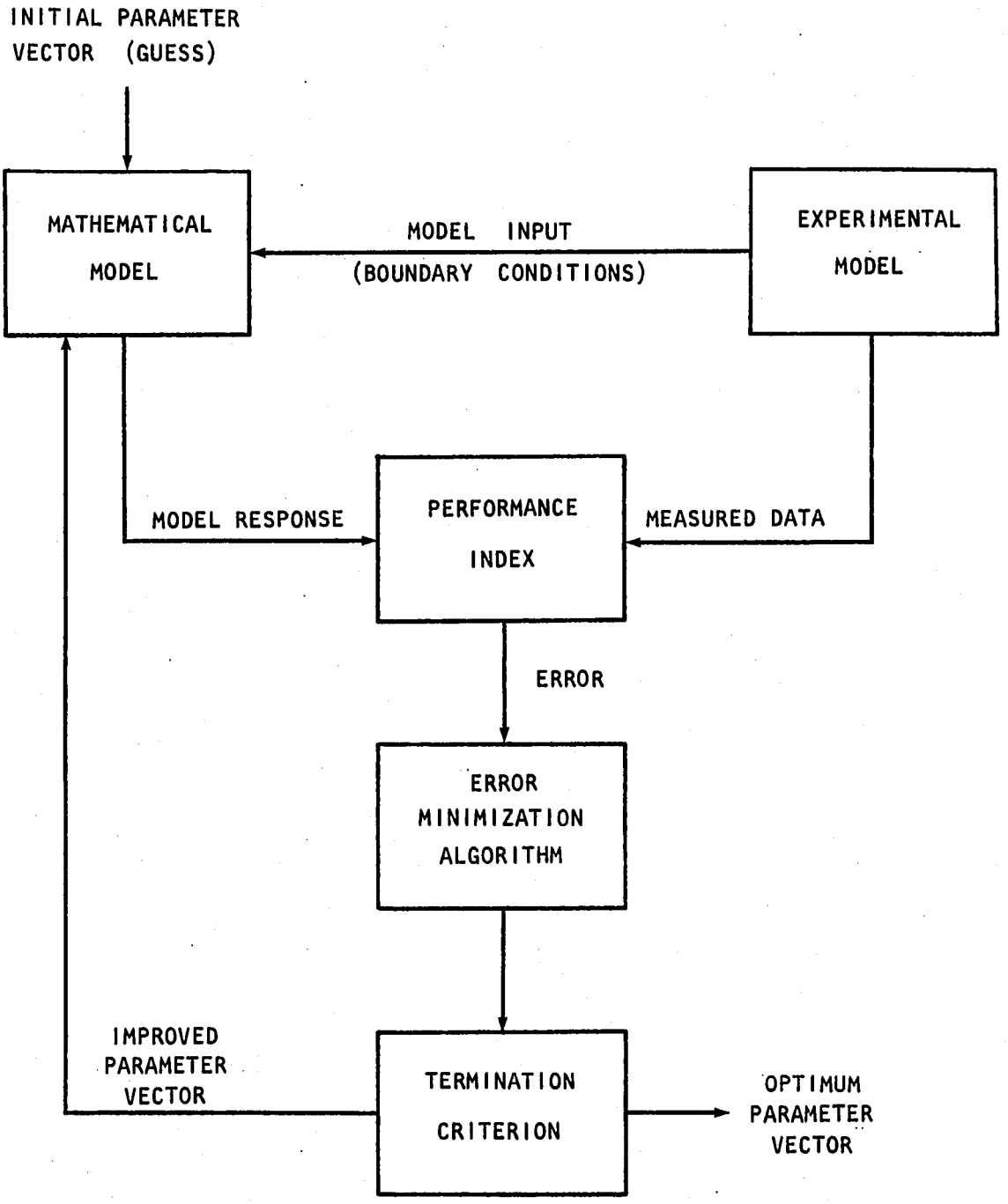
INITIAL PARAMETER VECTOR (GUESS)
MATHEMATICAL MODEL
MODEL INPUT (BOUNDARY CONDITIONS)
EXPERIMENTAL MODEL
MODEL RESPONSE
PERFORMANCE INDEX
MEASURED DATA
ERROR
ERROR MINIMIZATION ALGORITHM
IMPROVED PARAMETER VECTOR
TERMINATION CRITERION
OPTIMUM PARAMETER VECTOR

evaluate the following vessel and flow parameters: compliance C, radius R_o and peripheral resistance Z. In addition, if a stenosis was included in the mathematical model, the stenosis area ratio A_o/A_1 and the distance from the stenosis to either the proximal or distal end of the tube were estimated.

The mathematical model was used to provide input data of proximal pressure or flow and distal pressure, flow or resistance as boundary conditions. One or two of the remaining pressure or flow waveforms were used to provide observed data to form the performance index. This index was calculated as the sum of squared error between model response and measured data. All model parameters were directly measured experimentally so that values could be assigned to the model coefficients which were not to be estimated and so that the estimated parameters could be compared to measured values to assess the accuracy of the technique.

As described in Appendix B, the Gauss-Newton algorithm for minimizing a sum of squares is represented by the iterative scheme

$$\underline{b}^{(k+1)} = \underline{b}^{(k)} + ([X^{(k)}]^T[X^{(k)}])^{-1}([X^{(k)}]^T(\underline{Y} - \underline{y}^{(k)})) \qquad (5.1)$$

where superscripts refer to iteration number, $\underline{b}$ is the vector of parameter values, [X] is the matrix of sensitivity coefficients, and $\underline{Y}$ and $\underline{y}$ are the measured data and model response, respectively. In order to apply Equation 5.1 to the system of this study, let P(t) and Q(t) represent measured pressure and flow waveforms and let $p^{(k)}(t)$ and $q^{(k)}(t)$ denote the corresponding model results calculated using parameter values $\underline{b}^{(k)}$.

If both pressure and flow are used as observed variables in the parameter estimation procedure, define the vectors $\underline{Y}$ and $\underline{y}^{(k)}$ as follows:

$$Y_i = \begin{cases} P(t_i)/\bar{P}, & i = 1, 2, \ldots, N \\ Q(t_i)/\bar{Q}, & i = N+1, N+2, \ldots, 2N \end{cases} \tag{5.2}$$

$$y_i^{(k)} = \begin{cases} p^{(k)}(t_i)/\bar{P}, & i = 1, 2, \ldots, N \\ q^{(k)}(t_i)/\bar{Q}, & i = N+1, N+2, \ldots, 2N. \end{cases} \tag{5.3}$$

In Equations 5.2 and 5.3, $\bar{P}$ and $\bar{Q}$ are the mean measured pressure and flow, respectively, and $t_1, t_2, \ldots, t_N$ are a discrete set of times which span one "cardiac" cycle. The mean pressure and flow are used in these equations since the magnitudes of these waveforms differ by several orders of magnitude. A discrete set of times is used since the numerical solution scheme for the mathematical model produces such output. If only one waveform (either pressure or flow) is used in the estimation algorithm, normalized values are not necessary.

The performance index can now be computed as the sum of squared error between the vectors $\underline{Y}$ and $\underline{y}^{(k)}$,

$$S = (\underline{Y} - \underline{y}^{(k)})^T(\underline{Y} - \underline{y}^{(k)}) \equiv \sum_i (Y_i - y_i^{(k)})^2. \tag{5.4}$$

Other indices, such as the sum of absolute value error, can be used in parameter estimation algorithms, but Equation 5.4 is particularly well-suited to the Gauss-Newton minimization scheme and is commonly used.

In order to compute the sensitivity coefficient matrix [X] in Equation 5.1, the mathematical model is first solved using the parameter values $\underline{b}^{(k)}$. Next, the first component $b_1^{(k)}$ of the parameter vector is incremented by a small amount $\Delta b_1^{(k)}$ and the mathematical model is solved once more. The value $\Delta b_j^{(k)} = 0.001\ b_j^{(k)}$ was used in this study. This

process is repeated for each component of the parameter vector. The sensitivity coefficients are then approximated by

$$X_{ij}^{(k)} \equiv \frac{\partial y_i^{(k)}}{\partial b_j} = \frac{y(t_i, b_j^{(k)} + \Delta b_j^{(k)}) - y(t_i, b_j^{(k)})}{\Delta b_j^{(k)}} . \qquad (5.5)$$

The difference quotient in Equation 5.5 is calculated holding all components of the parameter vector equal to the values of $\underline{b}^{(k)}$ except for the component $b_j^{(k)}$.

The next step toward implementation of Equation 5.1 is inverting the sensitivity coefficient matrix $[X^{(k)}]$ calculated in Equation 5.5. There are two possibilities which may preclude this operation. First, if the mathematical model is not appreciably sensitive to one of the parameters, say b_j, then column j of the sensitivity matrix will be nearly zero and the inversion will fail. Another problem occurs if the sensitivity coefficients for two parameters, say b_j and b_n, are not independent. This will occur, for example, if $X_{ij}^{(k)} = aX_{in}^{(k)}$ where a is a constant. The matrix inversion will also fail under these conditions.

If these problems do not occur, Equation 5.1 will yield an improved parameter vector $\underline{b}^{(k+1)}$ in the sense that the sum of squares S in Equation 5.4 will have been reduced. In actual practice, due to numerical limitations of digital computation processes, the actual minimum value for S will not be achievable. Therefore, some criterion is required to terminate the algorithm when a stable parameter vector is obtained. The termination criterion chosen for this study is expressed as

$$\frac{|b_j^{(k+1)} - b_j^{(k)}|}{|b_j^{(k)}| + 10^{-20}} < 0.01 \qquad (5.6)$$

so that iterations cease if each component of $\underline{b}^{(k+1)}$ exhibits a change of less than one percent compared to the previous iteration. The term 10^{-20} in the denominator of Equation 5.6 is included to avoid numerical problems caused by the possibility of division by zero. This termination criterion also eliminates the problem of wasting computer time trying to estimate low sensitivity coefficients.

CHAPTER 6

RESULTS

The results of this study are discussed in four sections. First, the validity of the mathematical model is established by comparing calculated pressure and flow waveforms with those obtained experimentally. The experimental data are those obtained from the branched tube trial described in this thesis and straight tube results from previous research (Rooz, 1980). Second, once the applicability of the model has been verified, sensitivity of the measured waveforms to the parameters is established by solving the model equations with different parameter values and comparing the resulting waveforms. Third, the effectiveness of the parameter estimation scheme in determining system parameters is demonstrated by using model generated waveforms in place of experimental data as input. Finally, the parameter estimation scheme is used to produce estimates of various system parameters which are then compared with the corresponding directly measured values.

Validation of Mathematical Model

In order to validate the mathematical model, experimentally determined values were used for all system parameters and measured pressure or flow waveforms or peripheral resistance were used as boundary conditions. The waveforms which were not used as boundary conditions were then calculated and compared with the corresponding measured response. In this way, the overall performance of the model could be gauged and the validity of the modeling assumptions and numerical procedures ascertained.

First, the numerical approximation to the unconstricted straight tube model was checked. This process involved the investigation of the effect of choosing different combinations of boundary conditions (flow, pressure or peripheral resistance). Figures 6.1 through 6.3 show the results of imposing proximal flow-distal flow (Q-Q), proximal pressure-distal flow (P-Q) and proximal flow-peripheral resistance (Q-Z) boundary conditions. In each case, agreement between measured and calculated waveforms is good.

The "noise" in the calculated proximal flow using P-Q boundary conditions (Figure 6.2) is due primarily to the small number of elements in the finite element simulation used to produce the plots. A coarse finite element mesh was employed because of inefficiency of the numerical integration subroutine and limitations on computer time. Similar agreement was found with the combination of proximal pressure-peripheral resistance (P-Z) boundary conditions. However, proximal and distal pressure (P-P) as boundary conditions did not produce satisfactory results. This was caused by small errors in the experimental pressure measurements. Because of the strong influence of the pressure gradient upon the flow, small errors in pressure measurements produce significant errors in flow calculations.

Since the model equations for an unobstructed tube accurately reproduce the _in vitro_ data, the stenosis pressure drop Equation 3.12 can be inserted in order to assess its applicability. _In vitro_ data were obtained by Rooz (1980) which included a moderate (75 percent area reduction) or a severe (90 percent area reduction) stenosis in the form

Figure 6.1. Comparison between calculated and experimental pressures and flows for unobstructed straight tube. Q - Q boundary conditions. Parameters: $A_o = 0.35\ cm^2$, $C = 3.1 \times 10^{-7}\ cm^4/dyne$, $f = 0.62\ Hz$

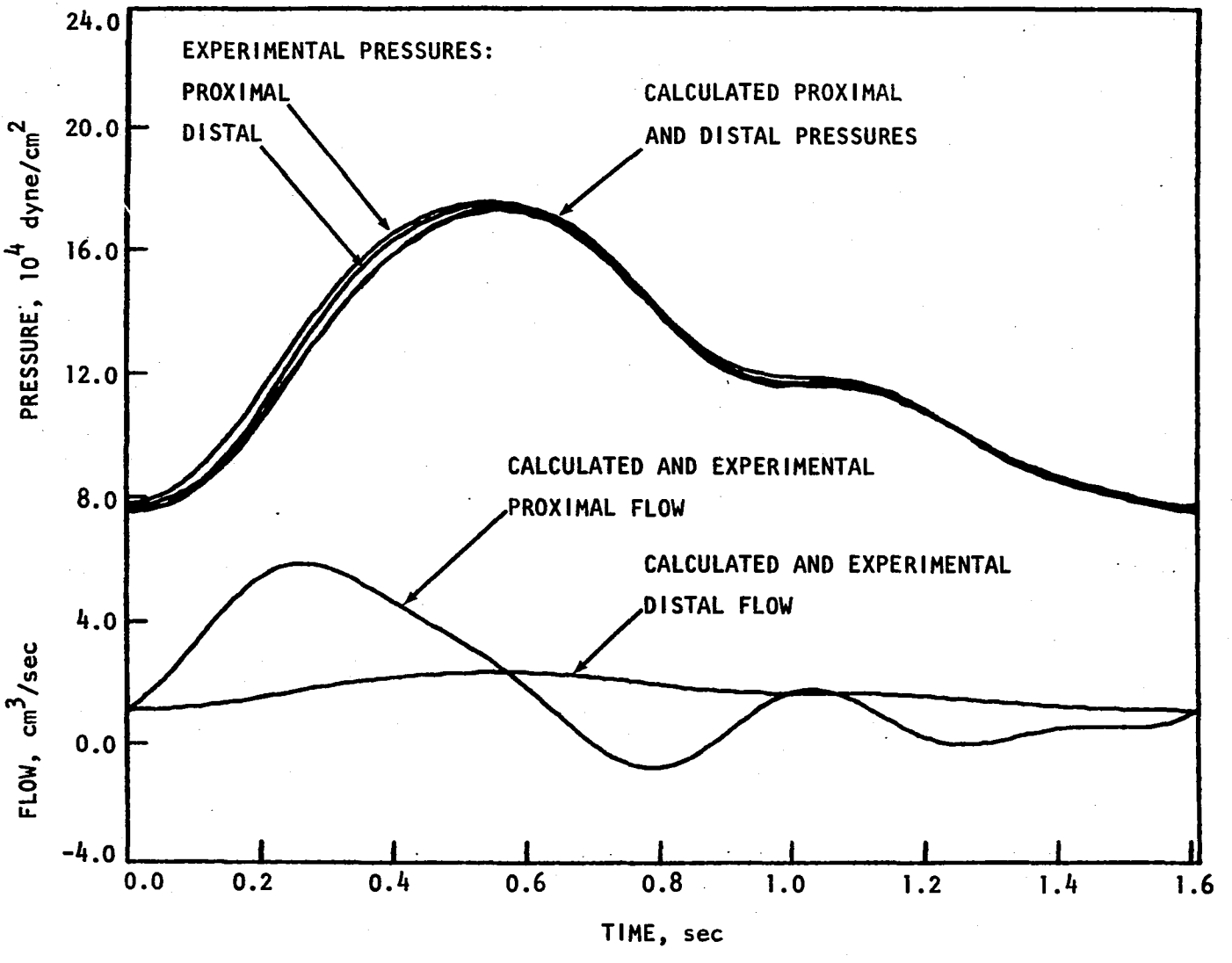
24.0
20.0
16.0
12.0
8.0
4.0
0.0
-4.0
PRESSURE, 10^4 dyne/cm^2
FLOW, cm^3/sec
EXPERIMENTAL PRESSURES:
PROXIMAL
DISTAL
CALCULATED PROXIMAL
AND DISTAL PRESSURES
CALCULATED AND EXPERIMENTAL
PROXIMAL FLOW
CALCULATED AND EXPERIMENTAL
DISTAL FLOW
0.0
0.2
0.4
0.6
0.8
1.0
1.2
1.4
1.6
TIME, sec

Figure 6.2. Comparison between calculated and experimental pressures and flows for unobstructed straight tube. P - Q boundary conditions. Parameters; $A_o = 0.35\ cm^2$, $C = 3.1 \times 10^{-7}\ cm^4/dyne$, $f = 0.62\ Hz$

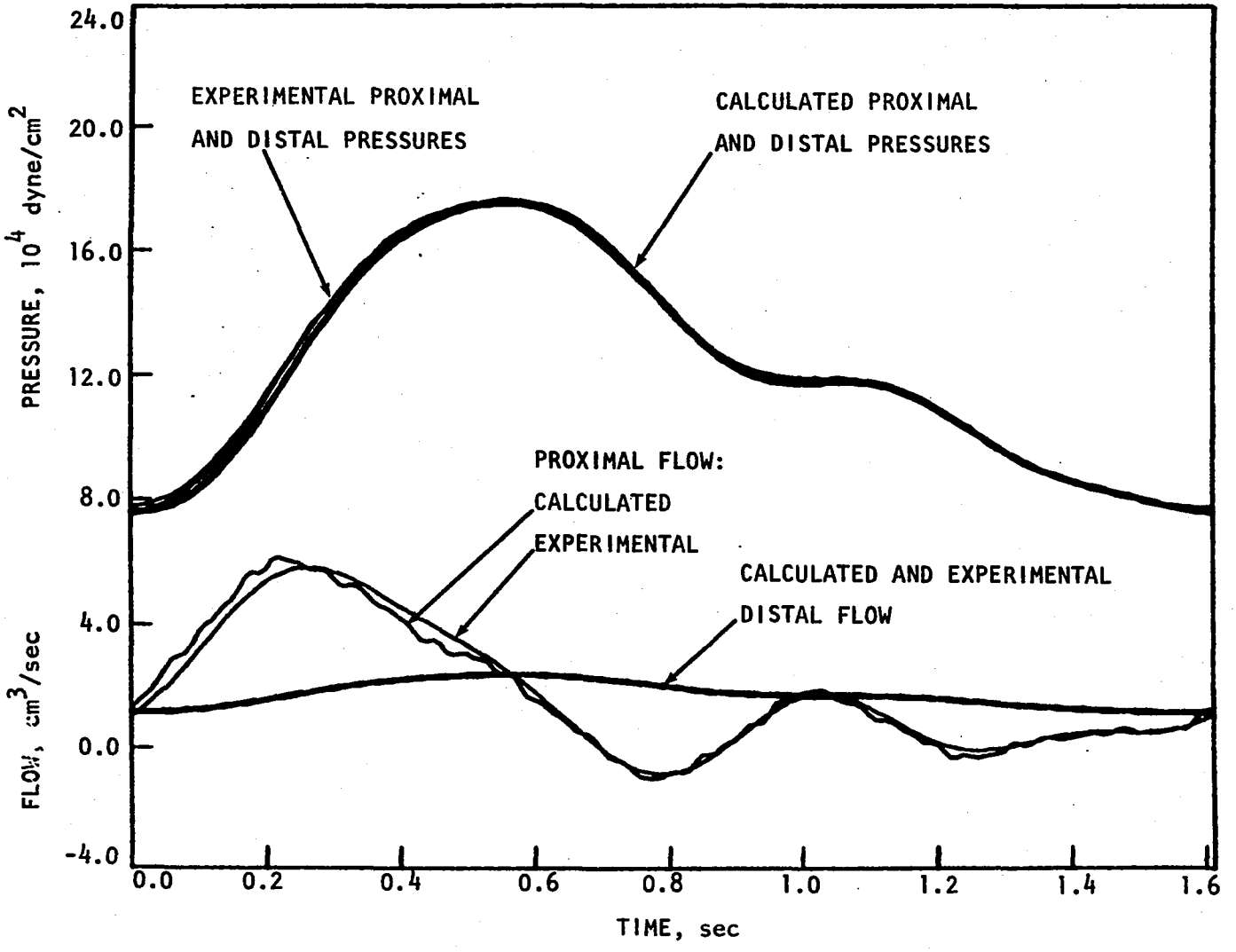
24.0
20.0
16.0
12.0
8.0
4.0
0.0
-4.0
PRESSURE, 10^4 dyne/cm^2
FLOW, cm^3/sec
EXPERIMENTAL PROXIMAL
AND DISTAL PRESSURES
CALCULATED PROXIMAL
AND DISTAL PRESSURES
PROXIMAL FLOW:
CALCULATED
EXPERIMENTAL
CALCULATED AND EXPERIMENTAL
DISTAL FLOW
0.0
0.2
0.4
0.6
0.8
1.0
1.2
1.4
1.6
TIME, sec

Figure 6.3. Comparison between calculated and experimental pressures and flows for unobstructed straight tube. Q - Z boundary conditions. Parameters: $A_o = 0.35\ cm^2$, $C = 3.1 \quad 10^{-7}\ cm^4/dyne$, $f = 0.62\ Hz$, $Z = 69300\ dyne\text{-}sec/cm^5$

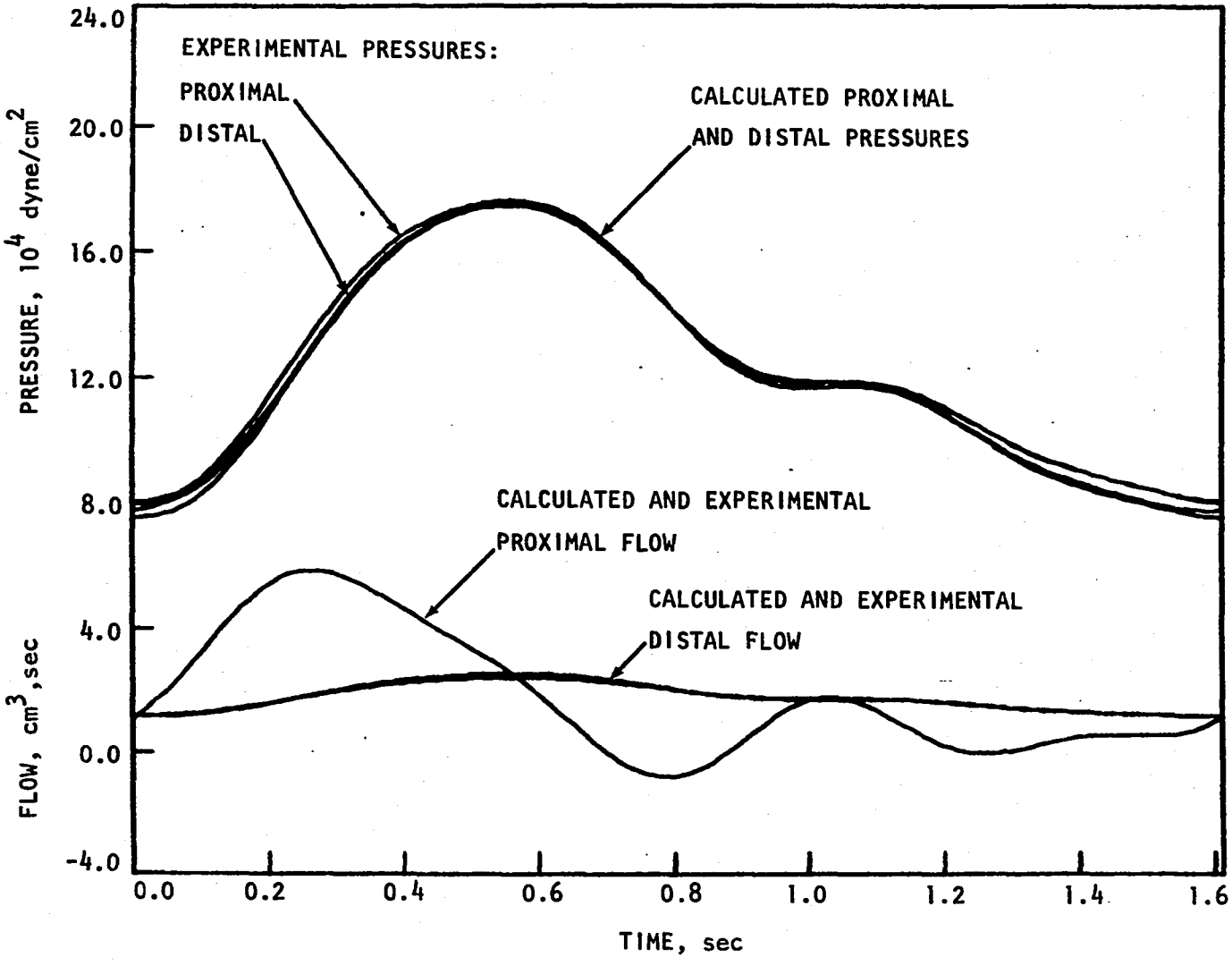
EXPERIMENTAL PRESSURES:
PROXIMAL
DISTAL
CALCULATED PROXIMAL
AND DISTAL PRESSURES
CALCULATED AND EXPERIMENTAL
PROXIMAL FLOW
CALCULATED AND EXPERIMENTAL
DISTAL FLOW
PRESSURE, 10^4 dyne/cm^2
FLOW, cm^3,sec
TIME, sec
24.0
20.0
16.0
12.0
8.0
4.0
0.0
-4.0
0.0
0.2
0.4
0.6
0.8
1.0
1.2
1.4
1.6

of a rigid axisymmetric blunt plug. The severe stenosis was located either at the center of the flexible tube or near the proximal end in order to provide variation due to stenosis position. Comparisons between measured and calculated waveforms are shown in Figures 6.4 through 6.6. As in the case of the unobstructed tube, a better match between experimental and numerical waveforms will be obtained by using a finer finite element mesh. However, limitations on computer time precluded this refinement. In spite of this, the agreement appears to be satisfactory.

As a final step toward validation of the mathematical model, branching flow using the relationships shown in Equations 3.9 and 3.10 was included. In order to reduce required input data to a minimum, the specified boundary conditions were proximal flow and two distal resistances (Q-Z-Z). The experimental model as described in Chapter 4 contained a 90 percent stenosis located proximal to the branch. Comparisons between measured and calculated waveforms are shown in Figures 6.7 through 6.10. The pressure waveforms are observed to match favorably, although there is significant difference between measured and calculated flow. This disparity is due in part to experimental error, since there are some errors involved in both the pressure and flow measurements, and to the assumption of constant resistance and compliance. In addition, the branch model equations may introduce errors.

Overall, it appeared that the mathematical model and finite element solution provided a satisfactory solution to pulsatile flow in both straight and branched tube flows, with and without stenoses.

Figure 6.4. Comparison between calculated and experimental proximal flows and distal pressures for straight tube with 75% stenosis midway between proximal and distal ends of tube. P - Q boundary conditions. Parameters: $A_o = 0.36\ cm^2$, $A_o/A_1 = 4.0$, $C = 2.7 \times 10^{-7}\ cm^4/dyne$, $f = 0.74$ Hz

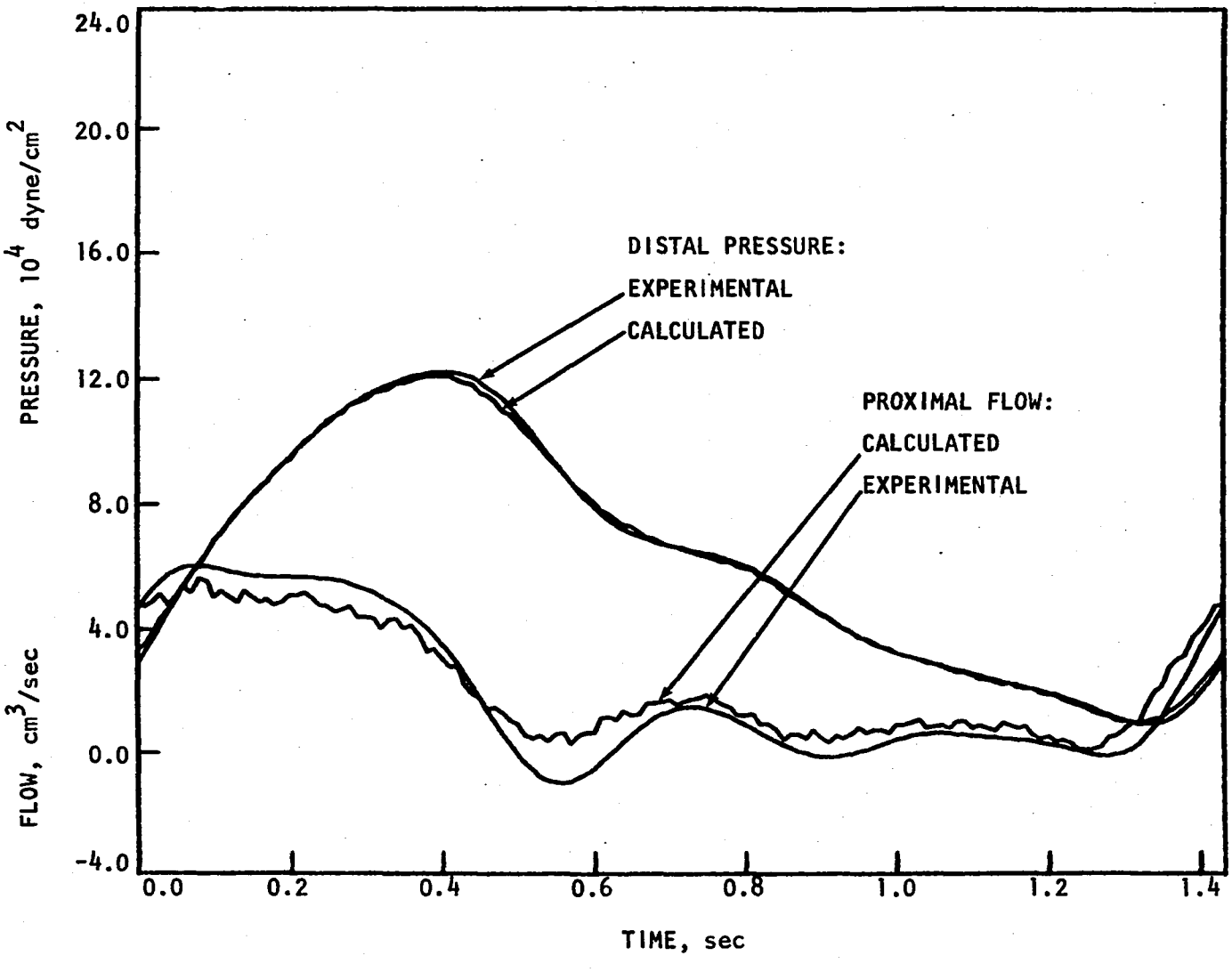
24.0
20.0
16.0
12.0
8.0
4.0
0.0
-4.0
PRESSURE, 10^4 dyne/cm^2
FLOW, cm^3/sec
DISTAL PRESSURE:
EXPERIMENTAL
CALCULATED
PROXIMAL FLOW:
CALCULATED
EXPERIMENTAL
0.0
0.2
0.4
0.6
0.8
1.0
1.2
1.4
TIME, sec

Figure 6.5. Comparison between calculated and experimental proximal flows and distal pressures for straight tube with 90% stenosis midway between proximal and distal ends of tube. P - Q boundary conditions. Parameters: $A_o = 0.36\ cm^2$, $A_o/A_1 = 10.0$, $C = 2.7 \times 10^{-7}\ cm^4/dyne$, $f = 1.03$ Hz

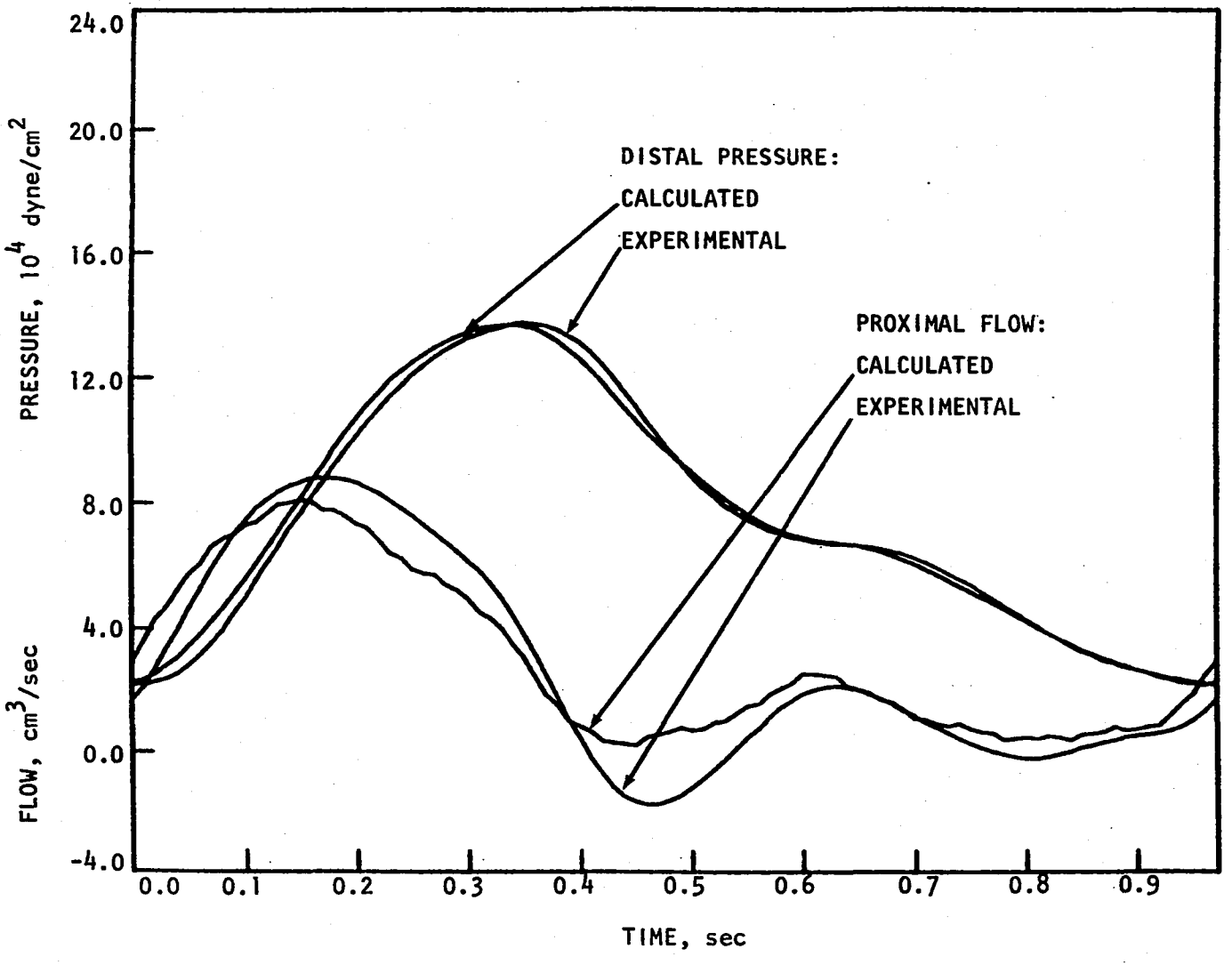
24.0
20.0
16.0
12.0
8.0
4.0
0.0
-4.0
PRESSURE, 10^4 dyne/cm^2
FLOW, cm^3/sec
DISTAL PRESSURE:
CALCULATED
EXPERIMENTAL
PROXIMAL FLOW:
CALCULATED
EXPERIMENTAL
0.0
0.1
0.2
0.3
0.4
0.5
0.6
0.7
0.8
0.9
TIME, sec

Figure 6.6. Comparison between calculated and experimental proximal flows and distal pressures for straight tube with 90% stenosis near proximal end of tube. P - Q boundary conditions. Parameters: $A_o = 0.36\ cm^2$, $A_o/A_1 = 10.0$, $C = 2.7 \times 10^{-7}\ cm^4/dyne$, $f = 1.03\ Hz$

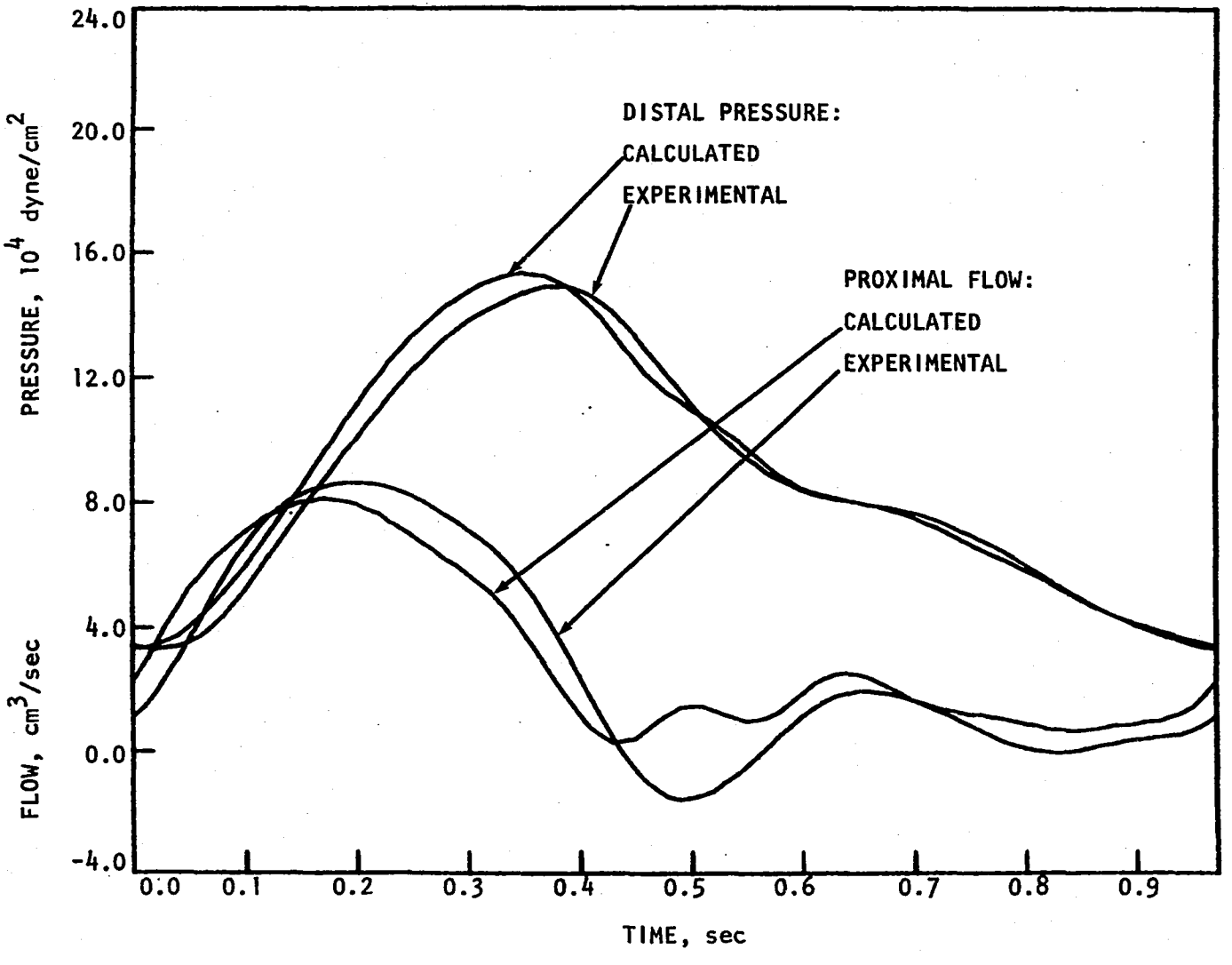
24.0
20.0
16.0
12.0
8.0
4.0
0.0
-4.0
PRESSURE, 10^4 dyne/cm^2
FLOW, cm^3/sec
DISTAL PRESSURE:
CALCULATED
EXPERIMENTAL
PROXIMAL FLOW:
CALCULATED
EXPERIMENTAL
0.0
0.1
0.2
0.3
0.4
0.5
0.6
0.7
0.8
0.9
TIME, sec

Figure 6.7. Comparison between calculated and experimental proximal pressures for branched tube with 90% stenosis upstream from branch. Q - Z - Z boundary conditions. Parameters: $A_p = 0.34$ cm^2, $A_p/A_1 = 10.0$, $A_d = A_b = 0.33$ cm^2, $C_p = 3.5 \times 10^{-7}$ cm^4/dyne, $C_d = C_b = 2.9 \times 10^{-7}$ cm^4/dyne, $Z_d = 20300$ dyne-sec/cm^5, $Z_b = 14000$ dyne-sec/cm^5, $f = 1.04$ Hz

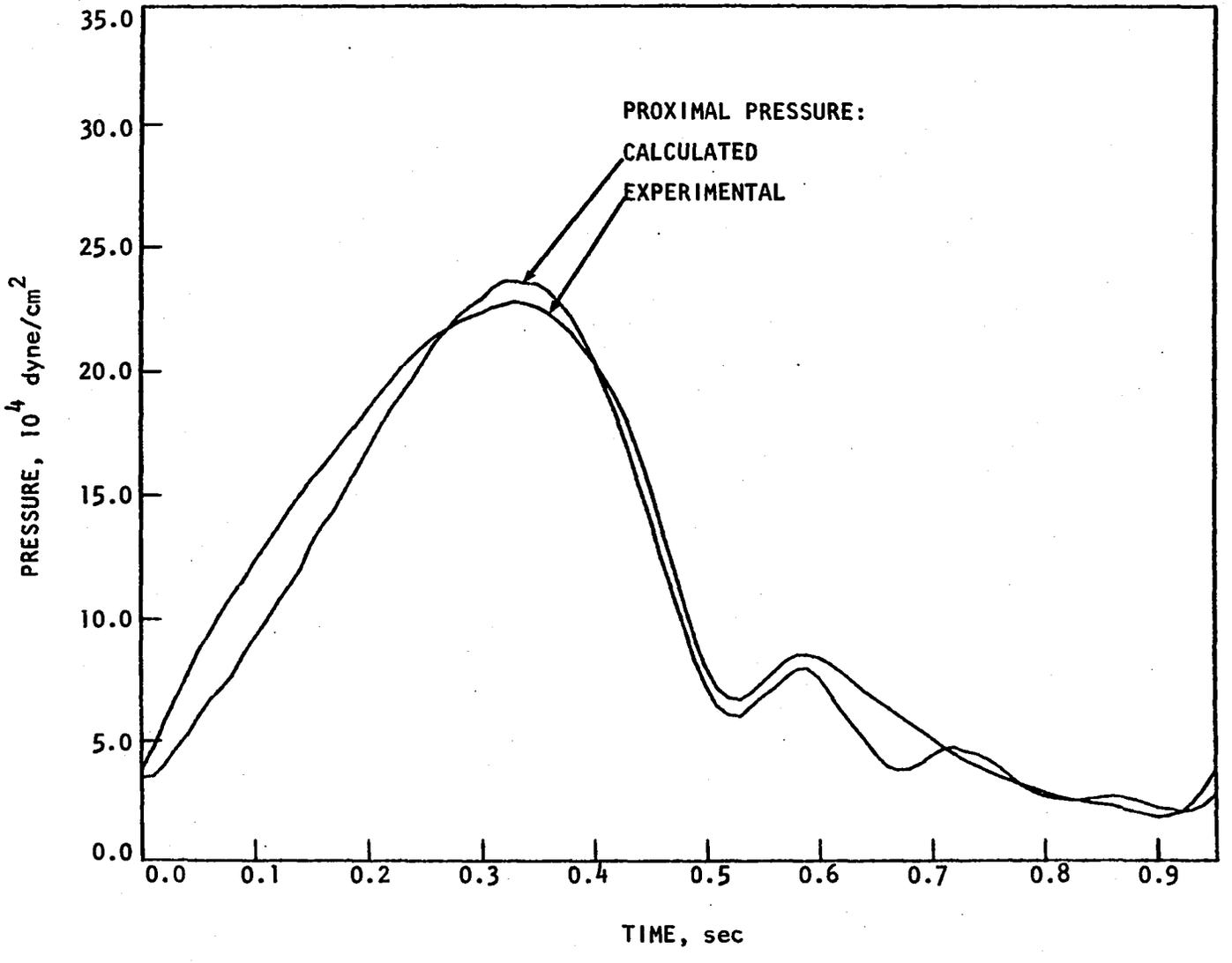
PROXIMAL PRESSURE:
CALCULATED
EXPERIMENTAL
PRESSURE, 10^4 dyne/cm^2
35.0
30.0
25.0
20.0
15.0
10.0
5.0
0.0
0.0
0.1
0.2
0.3
0.4
0.5
0.6
0.7
0.8
0.9
TIME, sec

Figure 6.8. Comparison between calculated and experimental distal flows for branched tube with 90% stenosis upstream from branch. Q - Z - Z boundary conditions. Parameters: $A_p = 0.34$ cm^4, $A_p/A_l = 10.0$, $A_d = A_b = 0.33$ cm^2, $C_p = 3.5 \times 10^{-7}$ cm^4/dyne, $C_d = C_b = 2.9 \times 10^{-7}$ cm^4/dyne, $Z_d = 20300$ dyne-sec/cm^5, $Z_b = 14000$ dyne-sec/cm^5, f = 1.04 Hz

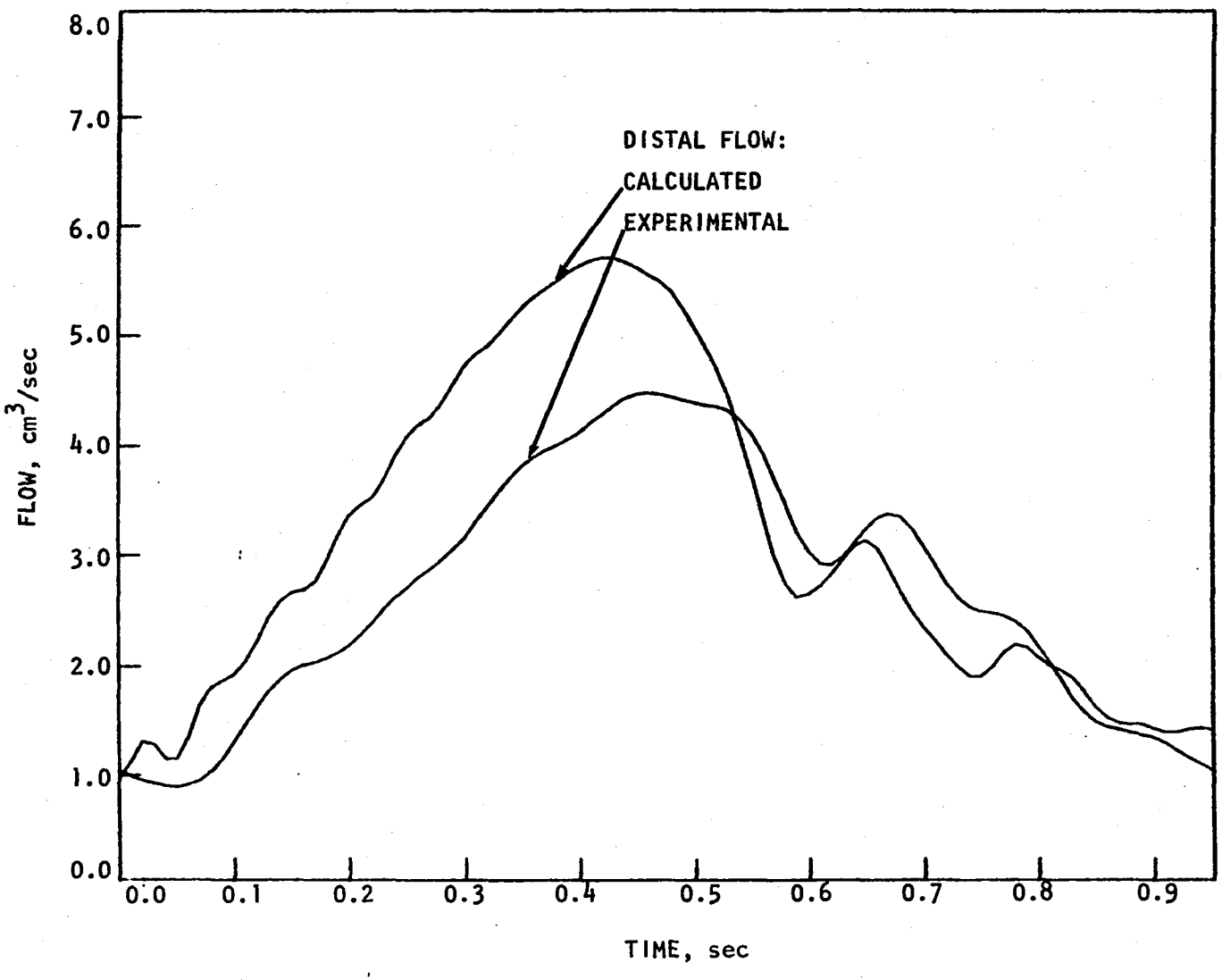
8.0
7.0
6.0
5.0
4.0
3.0
2.0
1.0
0.0
FLOW, cm³/sec
DISTAL FLOW:
CALCULATED
EXPERIMENTAL
0.0
0.1
0.2
0.3
0.4
0.5
0.6
0.7
0.8
0.9
TIME, sec

Figure 6.9. Comparison between calculated and experimental distal pressures for branched tube with 90% stenosis upstream from branch. Q - Z - Z boundary conditions. Parameters: $A_p = 0.34$ cm^2, $A_p/A_1 = 10.0$, $A_d = A_b = 0.33$ cm^2, $C_p = 3.5 \times 10^{-7}$ cm^4/dyne, $C_d = C_b = 2.9 \times 10^{-7}$ cm^4/dyne, $Z_d = 20300$ dyne-sec/cm^5, $Z_b = 14000$ dyne-sec/cm^5, f = 1.04 Hz

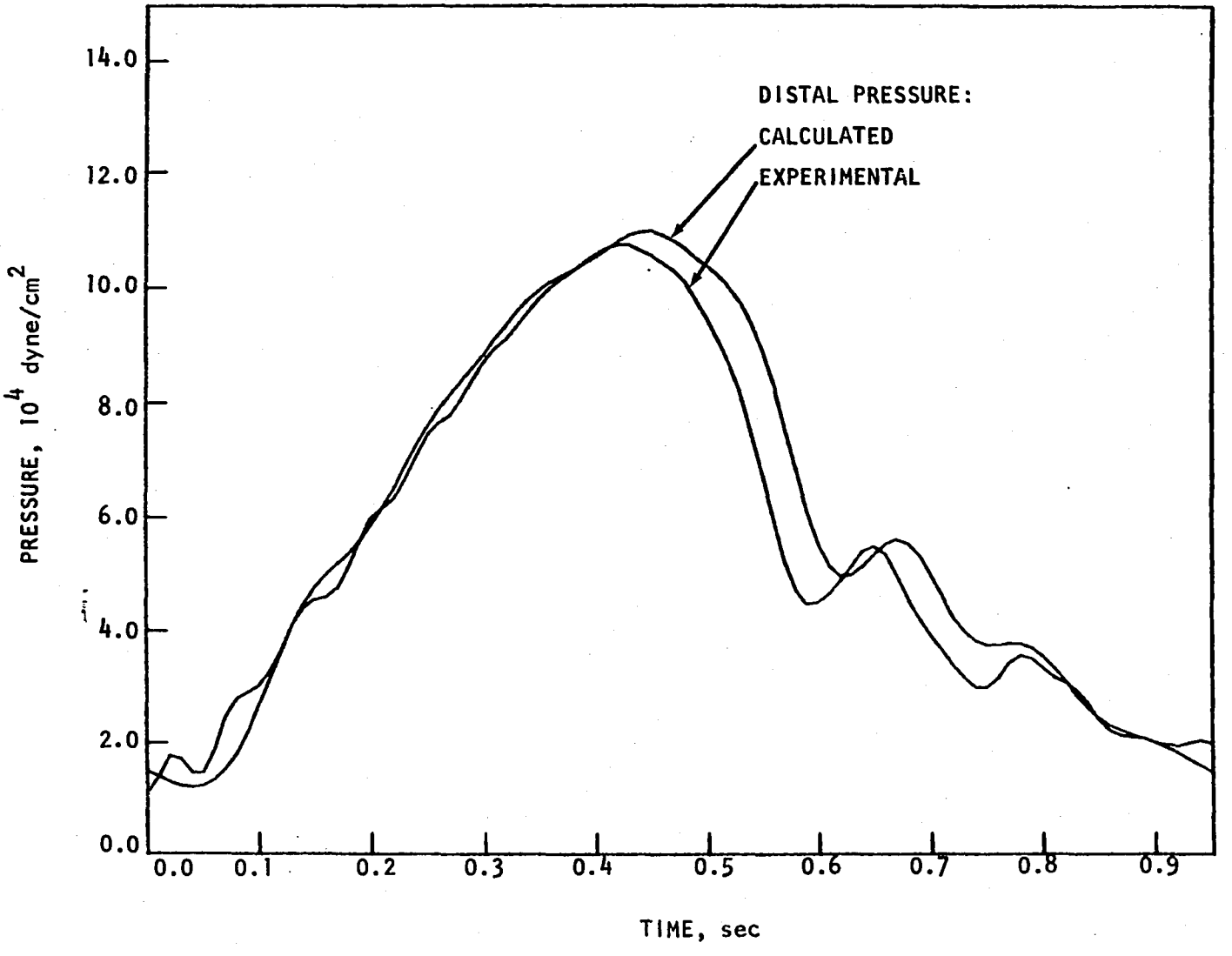
DISTAL PRESSURE:
CALCULATED
EXPERIMENTAL
PRESSURE, 10^4 dyne/cm^2
14.0
12.0
10.0
8.0
6.0
4.0
2.0
0.0
0.0
0.1
0.2
0.3
0.4
0.5
0.6
0.7
0.8
0.9
TIME, sec

Figure 6.10. Comparison between calculated and experimental branch pressures for branched tube with 90% stenosis upstream from branch. Q - Z - Z boundary conditions. Parameters: $A_p = 0.34$ cm^2, $A_p/A_1 = 10.0$, $A_d = A_b = 0.33$ cm^2, $C_p = 3.5 \times 10^{-7}$ cm^4/dyne, $C_d = C_b = 2.9 \times 10^{-7}$ cm^4/dyne, $Z_d = 20300$ dyne-sec/cm^5, $Z_b = 14000$ dyne-sec/cm^5, f = 1.04 Hz

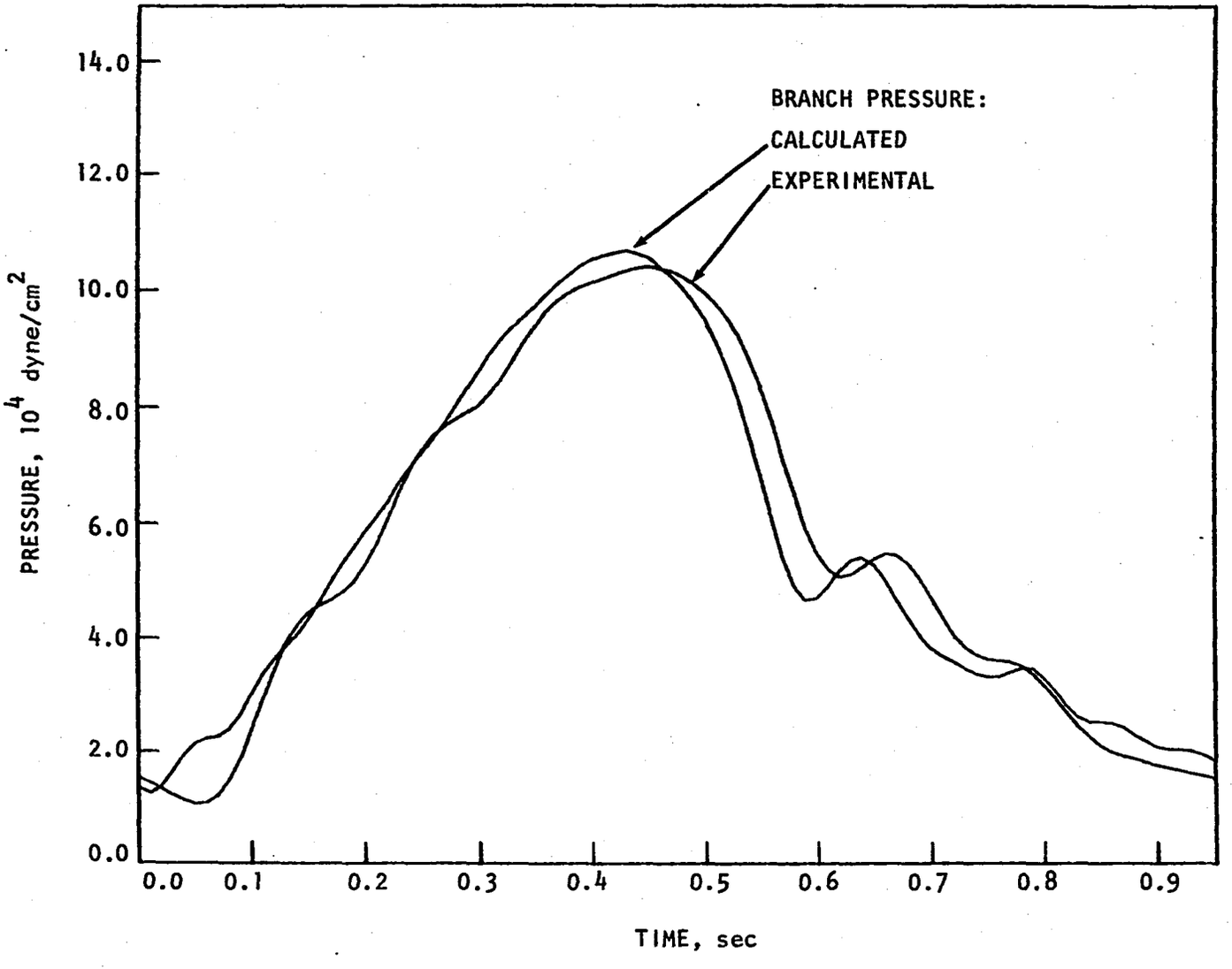
BRANCH PRESSURE:
CALCULATED
EXPERIMENTAL
PRESSURE, 10^4 dyne/cm^2
14.0
12.0
10.0
8.0
6.0
4.0
2.0
0.0
0.0
0.1
0.2
0.3
0.4
0.5
0.6
0.7
0.8
0.9
TIME, sec

Determination of Sensitivity of Parameters

The success of a scheme to estimate system parameters is strongly influenced by the sensitivity of the computed model response to those parameters. Thus, the mathematical model was used to study this sensitivity by calculating the variations in pressure and flow waveforms caused by changing the values of the system parameters. The parameters of interest included vessel compliance and radius, peripheral resistance, the ratio A_o/A_1 of unobstructed tube area to stenosis area, and the location of the stenosis relative to the distal measuring site.

Results of these sensitivity trials are shown in Figures 6.11 through 6.15. Significant changes in the waveforms were observed except in the case of variation of the vessel radius. This lack of sensitivity indicates that successful estimation of the radius may not be possible. However, determination of the remaining parameters appears promising.

Validation of Estimation Technique

The parameter estimation technique described in Chapter 5 was tested by using model generated waveforms as input in place of experimental data. This allows the determination of the efficacy of the method while controlling simulation errors. Thus, any mismatch between estimated parameter values and those used to produce the model input will be due to inaccuracies in the estimation algorithm.

A summary of the results of the model-to-model comparisons is contained in Table 6.1. The estimated parameter values represent the results of several estimation trials in which the unknown parameters

Figure 6.11. Sensitivity of calculated proximal pressure and distal flow due to variation of vessel compliance. Unobstructed straight tube. Q - Z boundary conditions

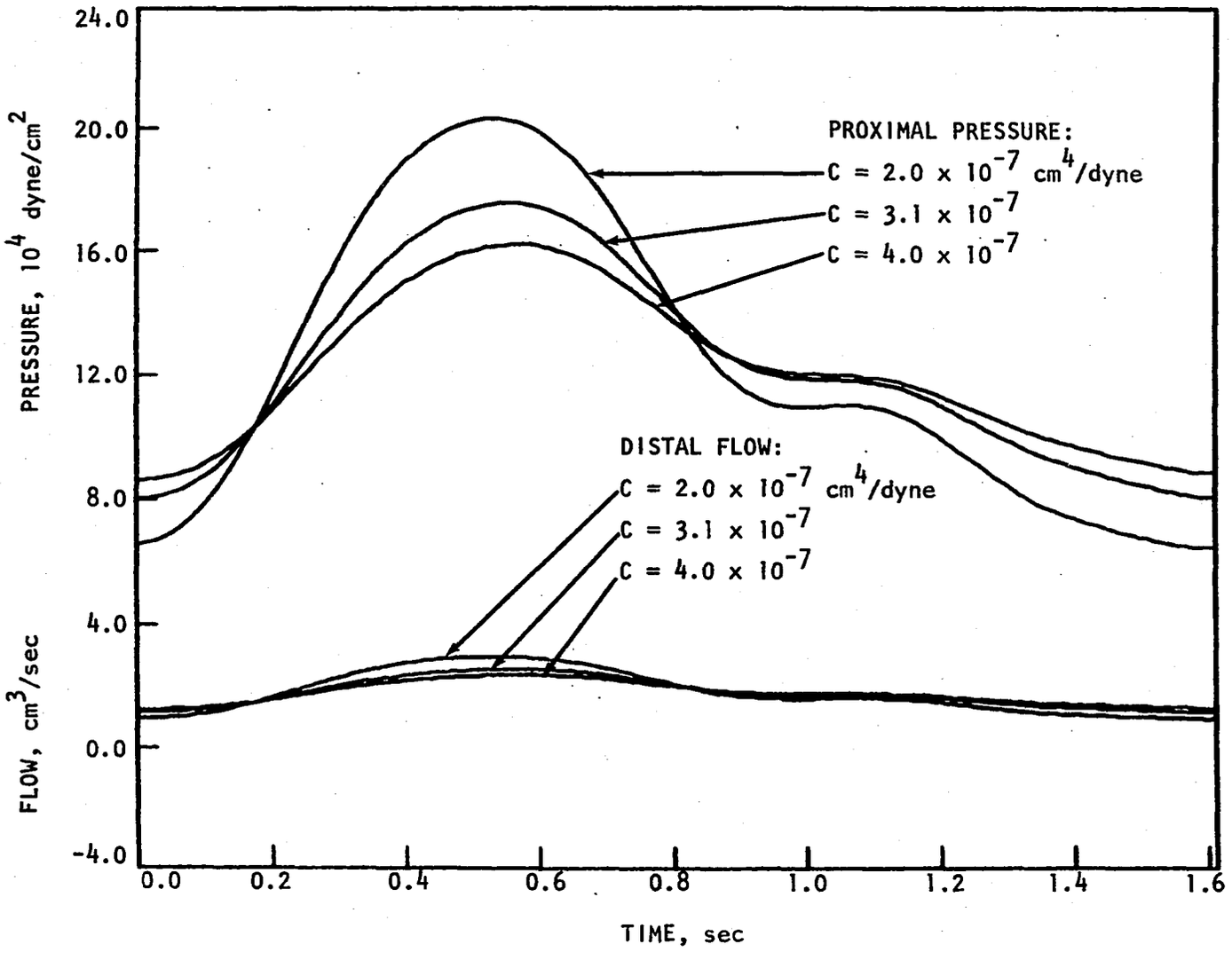
24.0
20.0
16.0
12.0
8.0
4.0
0.0
-4.0
PRESSURE, 10^4 dyne/cm^2
FLOW, cm^3/sec
PROXIMAL PRESSURE:
C = 2.0 x 10^{-7} cm^4/dyne
C = 3.1 x 10^{-7}
C = 4.0 x 10^{-7}
DISTAL FLOW:
C = 2.0 x 10^{-7} cm^4/dyne
C = 3.1 x 10^{-7}
C = 4.0 x 10^{-7}
0.0
0.2
0.4
0.6
0.8
1.0
1.2
1.4
1.6
TIME, sec

Figure 6.12. Sensitivity of calculated proximal pressure and distal flow due to variation of peripheral resistance. Unobstructed straight tube. Q - Z boundary conditions

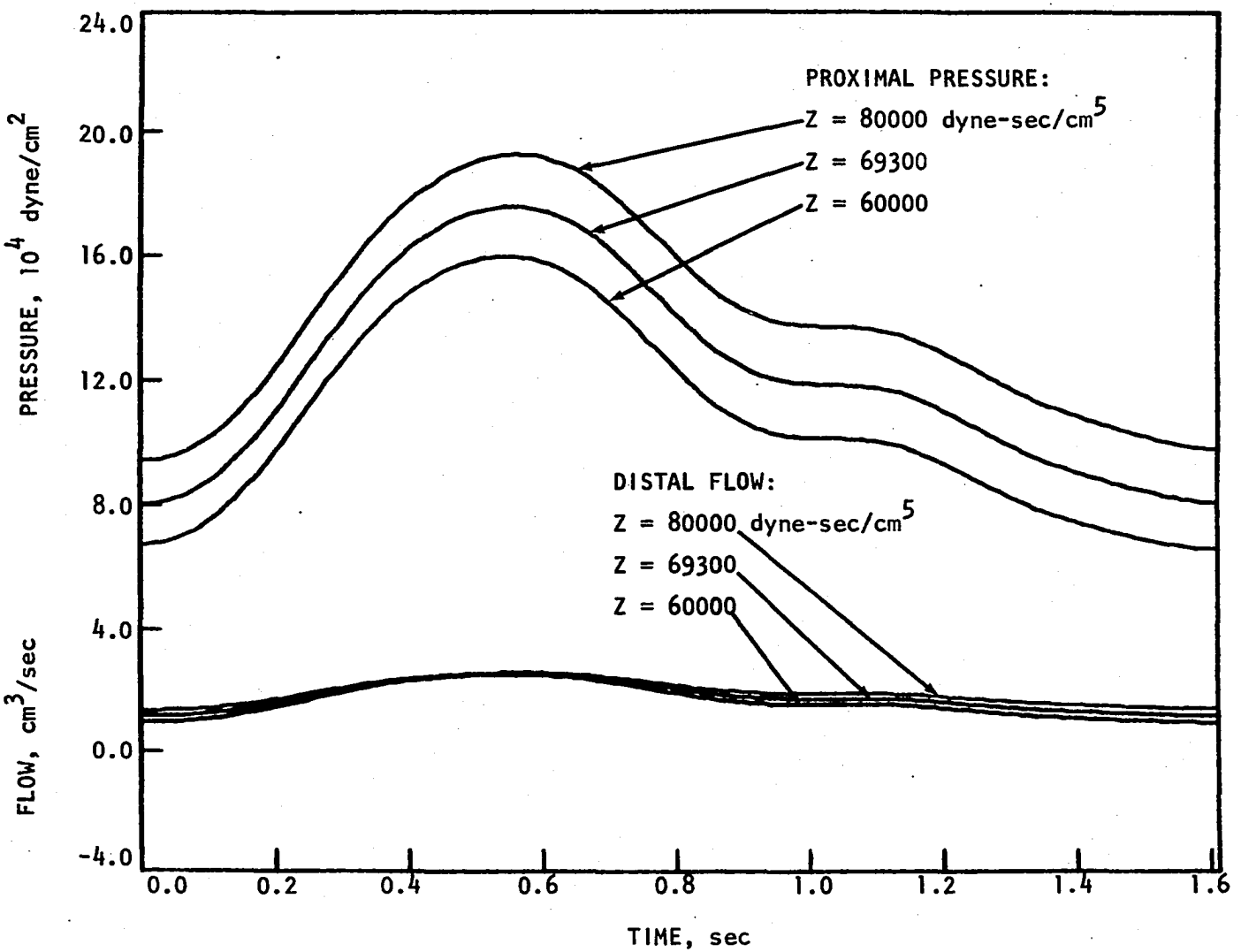
PROXIMAL PRESSURE:
Z = 80000 dyne-sec/cm5
Z = 69300
Z = 60000
DISTAL FLOW:
Z = 80000 dyne-sec/cm5
Z = 69300
Z = 60000
PRESSURE, 10^4 dyne/cm^2
FLOW, cm^3/sec
TIME, sec
24.0
20.0
16.0
12.0
8.0
4.0
0.0
-4.0
0.0
0.2
0.4
0.6
0.8
1.0
1.2
1.4
1.6

Figure 6.13. Sensitivity of calculated proximal pressure and distal flow due to variation in vessel radius. Unobstructed straight tube. Q - Z boundary conditions

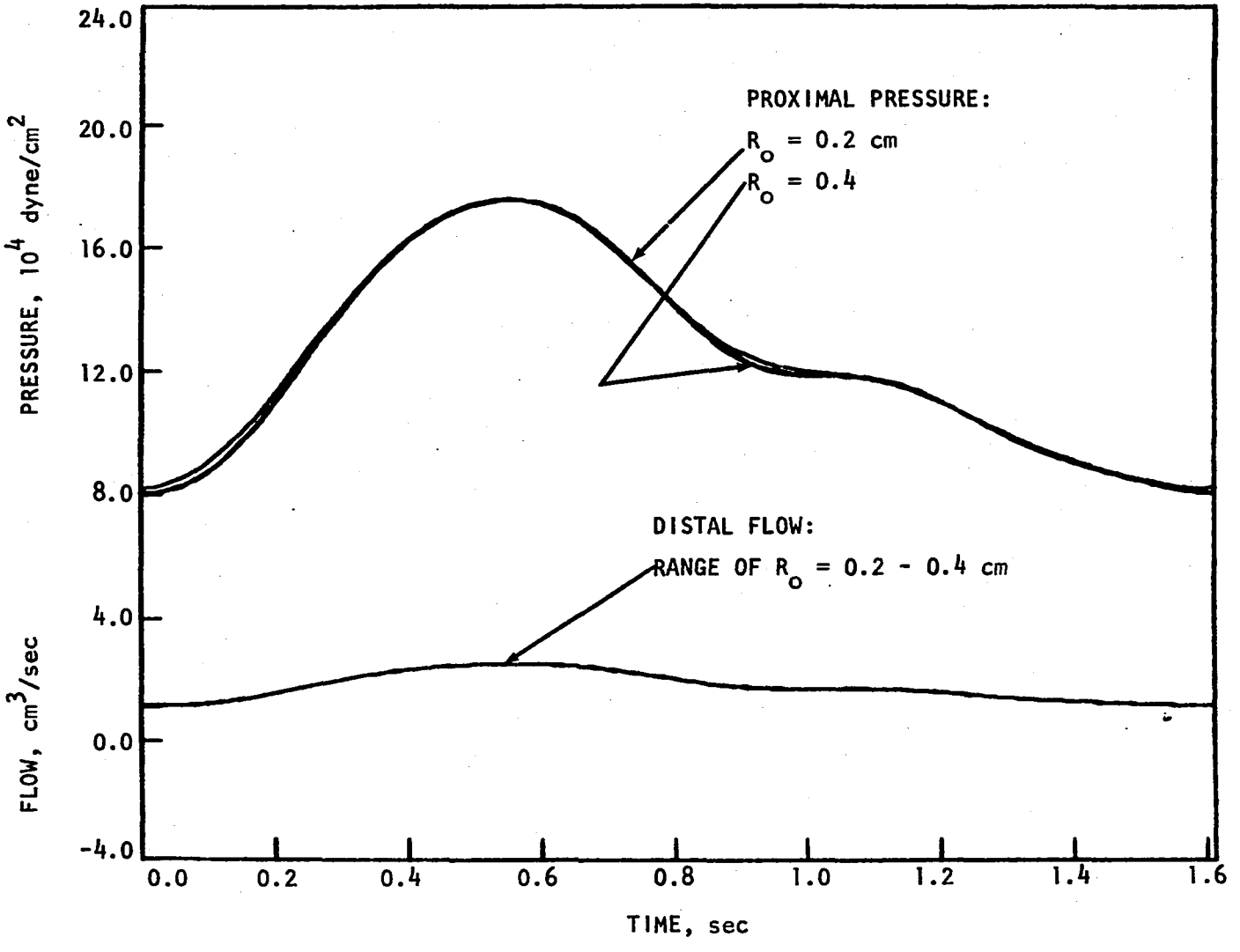
24.0
20.0
16.0
12.0
8.0
4.0
0.0
-4.0
PRESSURE, 10^4 dyne/cm^2
FLOW, cm^3/sec
PROXIMAL PRESSURE:
R_o = 0.2 cm
R_o = 0.4
DISTAL FLOW:
RANGE OF R_o = 0.2 - 0.4 cm
0.0
0.2
0.4
0.6
0.8
1.0
1.2
1.4
1.6
TIME, sec

Figure 6.14. Sensitivity of calculated distal pressure and proximal flow due to variation of area ratio. Straight tube with stenosis midway between proximal and distal ends of tube. P - Q boundary conditions

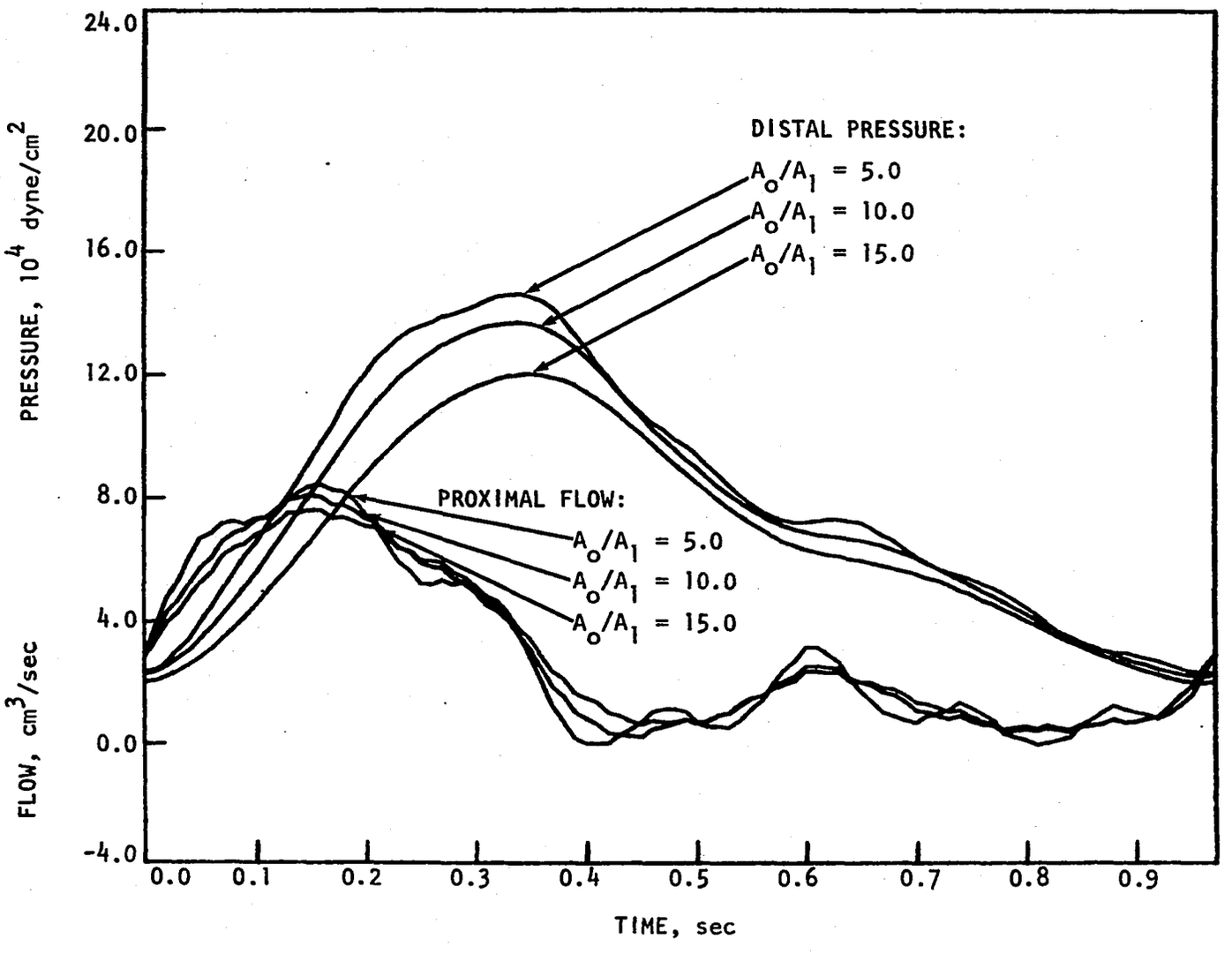
24.0
20.0
16.0
12.0
8.0
4.0
0.0
-4.0
PRESSURE, 10^4 dyne/cm^2
FLOW, cm^3/sec
DISTAL PRESSURE:
A_o/A_1 = 5.0
A_o/A_1 = 10.0
A_o/A_1 = 15.0
PROXIMAL FLOW:
A_o/A_1 = 5.0
A_o/A_1 = 10.0
A_o/A_1 = 15.0
0.0
0.1
0.2
0.3
0.4
0.5
0.6
0.7
0.8
0.9
TIME, sec

Figure 6.15. Sensitivity of calculated distal pressure and proximal flow due to variation of stenosis location. Straight tube with 90% stenosis midway between proximal and distal ends of tube. P - Q boundary conditions

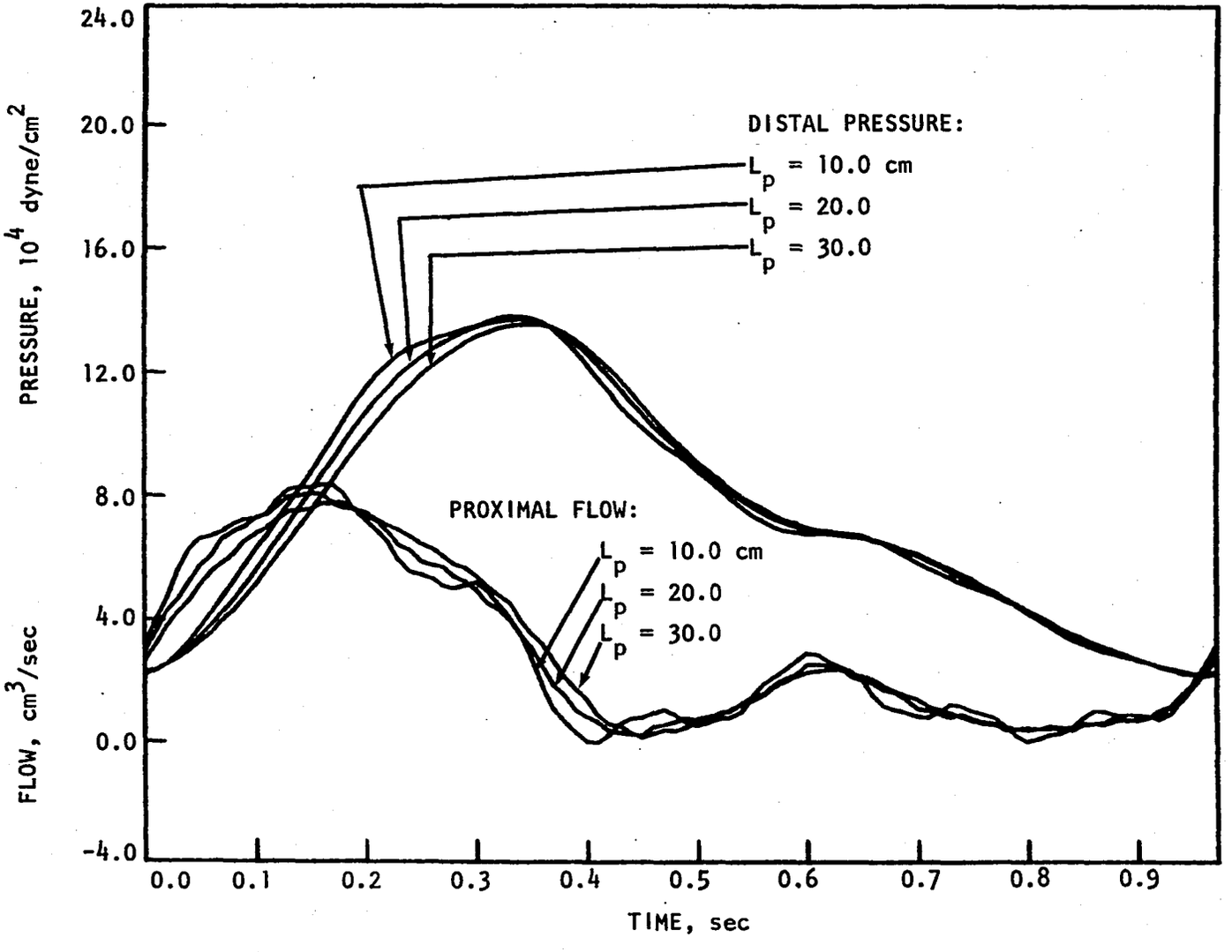
24.0
20.0
16.0
12.0
8.0
4.0
0.0
-4.0
PRESSURE, 10^4 dyne/cm^2
FLOW, cm^3/sec
DISTAL PRESSURE:
L_p = 10.0 cm
L_p = 20.0
L_p = 30.0
PROXIMAL FLOW:
L_p = 10.0 cm
L_p = 20.0
L_p = 30.0
0.0
0.1
0.2
0.3
0.4
0.5
0.6
0.7
0.8
0.9
TIME, sec

Table 6.1. Summary of model to model parameter estimation results

Model	Boundary Conditions	Observed[a] Variables	Parameters	Measured[b] Values	Estimated Values	Error[c]
Straight Tube	Q - Q	P_p	C	3.1×10^{-7}	3.1×10^{-7}	0
	Q - Z	P_p	Z	69300	69300	0
	Q - Z	P_p	C	3.1×10^{-7}	3.1×10^{-7}	0
			Z	69300	69300	0
Straight Tube with Central 75% Stenosis	P - Q	Q_p and P_d	A_o/A_1	4.0	4.0	0
	P - Q	Q_p and P_d	L_d	23.3	*[d]	*
Straight Tube with Central 90% Stenosis	P - Q	Q_p and P_d	A_o/A_1	10.0	10.0	0
	P - Q	Q_p and P_d	L_d	23.3	23.3	0
	P - Q	Q_p and P_d	A_o/A_1	10.0	10.0	0
			L_d	23.3	23.4	-0.4
Straight Tube with Proximal 90% Stenosis	P - Q	Q_p and P_d	A_o/A_1	10.0	10.0	0
	P - Q	Q_p and P_d	L_d	38.0	38.0	0
	P - Q	Q_p and P_d	A_o/A_1	10.0	10.0	0
			L_d	38.0	38.4	-1.1

[a] Observed variables are P_p = proximal pressure, P_d = distal pressure, or Q_p = proximal flow.

[b] Compliance, C - cm^4/dyne; resistance, Z - dyne-sec/cm^5; distal length, L_d - cm.

[c] Percent error = ((measured value - estimated value)/(measured value)) x 100.

[d] Could not be estimated.

were initialized to various starting values. Due to the low sensitivity to vessel radius, this parameter was not estimated.

For the straight tube model, trials were run using either Q-Q or Q-Z boundary conditions with proximal pressure used to determine the performance index. Since the peripheral resistance is not applicable when Q-Q boundary conditions are specified, only the vessel compliance was estimated in this case. It was found that the compliance and resistance could be accurately estimated individually or in combination.

The stenosed straight tube model was used to estimate the area ratio A_o/A_1 and the distance L_d measured from the stenosis to the distal measurement site. The boundary conditions P-Q were specified and the combination of proximal flow and distal pressure normalized by mean values was used to compute the residual error. In preliminary estimation trials, the distal pressure alone was used to determine the performance index. The two stenosis parameters could be estimated individually in this case, but the algorithm did not converge when estimating both simultaneously. This is thought to be caused by non-independence of parameter effects upon the pressure waveform. For a 90 percent stenosis, the area ratio and stenosis location could be accurately estimated individually or in combination. However, L_d could not be estimated for a mild (75 percent) stenosis. Subsequent analysis of waveforms assuming a 75 percent stenosis showed no visible variation due to changes in stenosis location. Thus, lack of sensitivity prevented estimation of L_d in this case.

Estimation of System Parameters

The mathematical model has been shown to produce satisfactory reproduction of the experimental data and to exhibit sensitivity to compliance, resistance, stenosis location and area ratio. Model-to-model comparisons have shown that the parameter estimation technique provides reliable values for the parameters of interest. It remains to be shown that the estimation method can successfully extract the desired parameters from experimental data.

The results for a straight tube are presented in Table 6.2. For purposes of comparison, the same combinations of boundary conditions and observed variables as in the model-to-model results in Table 6.1 were used. As expected, the estimated values of the parameters do not agree with the measured values as well as in the model-to-model comparisons. However, in most cases the difference between predicted and measured values is within ten percent.

This estimation error is caused primarily by two factors. First, modeling assumptions, such as constant vessel compliance, produce simulation error. That is, the mathematical model is not a perfect representation of the physical system. The second major factor is numerical error caused by a coarse finite element mesh. In particular, the unobstructed straight tube equations were solved using only eight equally spaced nodes and only five nodes proximal and distal to the stenosis were used in the solution to the stenosed tube model. Better agreement between measured and experimental waveforms would result from a finer mesh, but at the expense of longer computation times.

Table 6.2. Summary of model to experiment parameter estimation results for straight tube

Model	Boundary Conditions	Observed[a] Variables	Parameters	Measured[b] Values	Estimated Values	Error[c]
Straight Tube	Q - Q	P_p	C	3.1×10^{-7}	2.8×10^{-7}	9.7
	Q - Z	P_p	Z	69300	69000	0.4
	Q - Z	P_p	C	3.1×10^{-7}	2.9×10^{-7}	6.5
			Z	69300	68900	0.6
Straight Tube with Central 75% Stenosis	P - Q	Q_p and P_d	A_o/A_1	4.0	4.5	-12.5
	P - Q	Q_p and P_d	L_d	23.3	*[d]	*
Straight Tube with Central 90% Stenosis	P - Q	Q_p and P_d	A_o/A_1	10.0	11.0	-10.0
	P - Q	Q_p and P_d	L_d	23.3	27.1	-16.3
	P - Q	Q_p and P_d	A_o/A_1	10.0	9.1	9.0
			L_d	23.3	25.6	-9.9
Straight Tube with Proximal 90% Stenosis	P - Q	Q_p and P_d	A_o/A_1	10.0	9.9	1.0
	P - Q	Q_p and P_d	L_d	38.0	35.8	5.8
	P - Q	Q_p and P_d	A_o/A_1	10.0	10.1	-1.0
			L_d	38.0	40.1	-5.5

[a] Observed variables are P_p = proximal pressure, P_d = distal pressure, or Q_p = proximal flow.

[b] Compliance, C - cm^4/dyne; resistance, Z - dyne-sec/cm^5; distal length, L_d - cm.

[c] Percent error = ((measured value - estimated value)/(measured value)) x 100.

[d] Could not be estimated.

The results of the parameter estimation trials in conjunction with the branched model with stenosis are given in Table 6.3. Since the experimental model consisted of three separate lengths of tubing, a complete characterization of the system would require three compliance and two peripheral resistance values. However, due to computation time limitations, only the compliance of the tube proximal to the branch and the resistance for the main tube were estimated (Figure 3.1b). These parameters are indicated as C and Z, respectively, in Table 3. In addition, the position of the stenosis was determined by the length L_p of tube proximal to the stenosis.

Determination of compliance and area ratio individually produced reasonable estimates, although the error in the resistance was substantial. This is because the assumption of a constant resistance is not valid for the data obtained from the branched tube experiment. In the straight tube experiments, the distal resistance consisted of several small-diameter tubes in parallel and the ratio of instantaneous pressure to flow remained essentially constant. This resistance was not used in the branched trials. The values for area ratio and stenosis location were estimated simultaneously with less than 15 percent error. Finally, all four parameters were estimated with excellent agreement between measured and calculated stenosis properties, although once again the resistance estimate showed appreciable error. The compliance was determined to within 11 percent.

The efficiency of the parameter estimation scheme in reducing the residual error can be monitored by observing the progressive variation

Table 6.3. Summary of model to experiment parameter estimation results for branched tube

Model	Boundary Conditions	Observed[a] Variables	Parameters	Measured[b] Values	Estimated Values	Error[c]
Branched Tube with 90% Stenosis	Q - Z - Z	P_p and Q_d	C	3.5×10^{-7}	3.0×10^{-7}	14.3
	Q - Z - Z	P_p and Q_d	Z	20300	29700	-46.3
	Q - Z - Z	P_p and Q_d	A_o/A_1	10.0	10.8	-8.0
	Q - Z - Z	P_p and Q_d	A_o/A_1	10.0	10.4	-4.0
			L_p	27.5	23.6	14.2
	Q - Z - Z	P_p and Q_d	C	3.5×10^{-7}	3.1×10^{-7}	11.4
			Z	20330	26200	-29.1
			A_o/A_1	10.0	10.1	-1.0
			L_p	27.5	27.2	1.1

[a]Observed variables are P_p = proximal pressure, Q_d = distal flow.

[b]Compliance, C - cm^4/dyne; resistance, Z - dyne-sec/cm^5; distal length, L_d - cm.

[c]Percent error = ((measured value - estimated value)/(measured value)) x 100.

of the observed waveforms due to parameter improvement. Figures 6.16 and 6.17 show the variation of the proximal pressure and distal flow waveforms for the branched tube model with a 90 percent stenosis. The estimated parameters were the stenosis location and area ratio, compliance of the proximal tube segment, and peripheral resistance for the distal tube.

In both figures, the waveforms generated using parameter values from the second iteration of the estimation algorithm show little difference from the final converged values (eighth iteration). The measured waveforms are included on these figures for comparison. The parameter values which resulted from this estimation trial and which were used to produce Figures 6.16 and 6.17 are given in Table 6.4.

Table 6.4. Parameter values during iterations of estimation procedure for results shown in Figures 6.16 and 6.17

	Parameters			
Iteration	Compliance C_p [a]	Resistance Z_d [b]	Area Ratio A_p/A_1	Stenosis Location L_p [c]
0	2.0×10^{-7}	15000	15.0	20.0
1	2.5×10^{-7}	23000	10.8	23.5
2	3.2×10^{-7}	26400	10.0	23.9
3	3.4×10^{-7}	26500	10.0	24.5
4	3.4×10^{-7}	26300	10.1	25.0
5	3.2×10^{-7}	26300	10.1	26.6
6	3.2×10^{-7}	26200	10.1	26.9
7	3.1×10^{-7}	26200	10.1	27.2
8	3.1×10^{-7}	26200	10.1	27.3

[a] Compliance - cm^2/dyne.
[b] Resistance - dyne-sec/cm^5.
[c] Stenosis location - cm.

Figure 6.16. Convergence of calculated proximal pressure waveforms from parameter estimation trial. Branched tube with 90% stenosis upstream from branch.

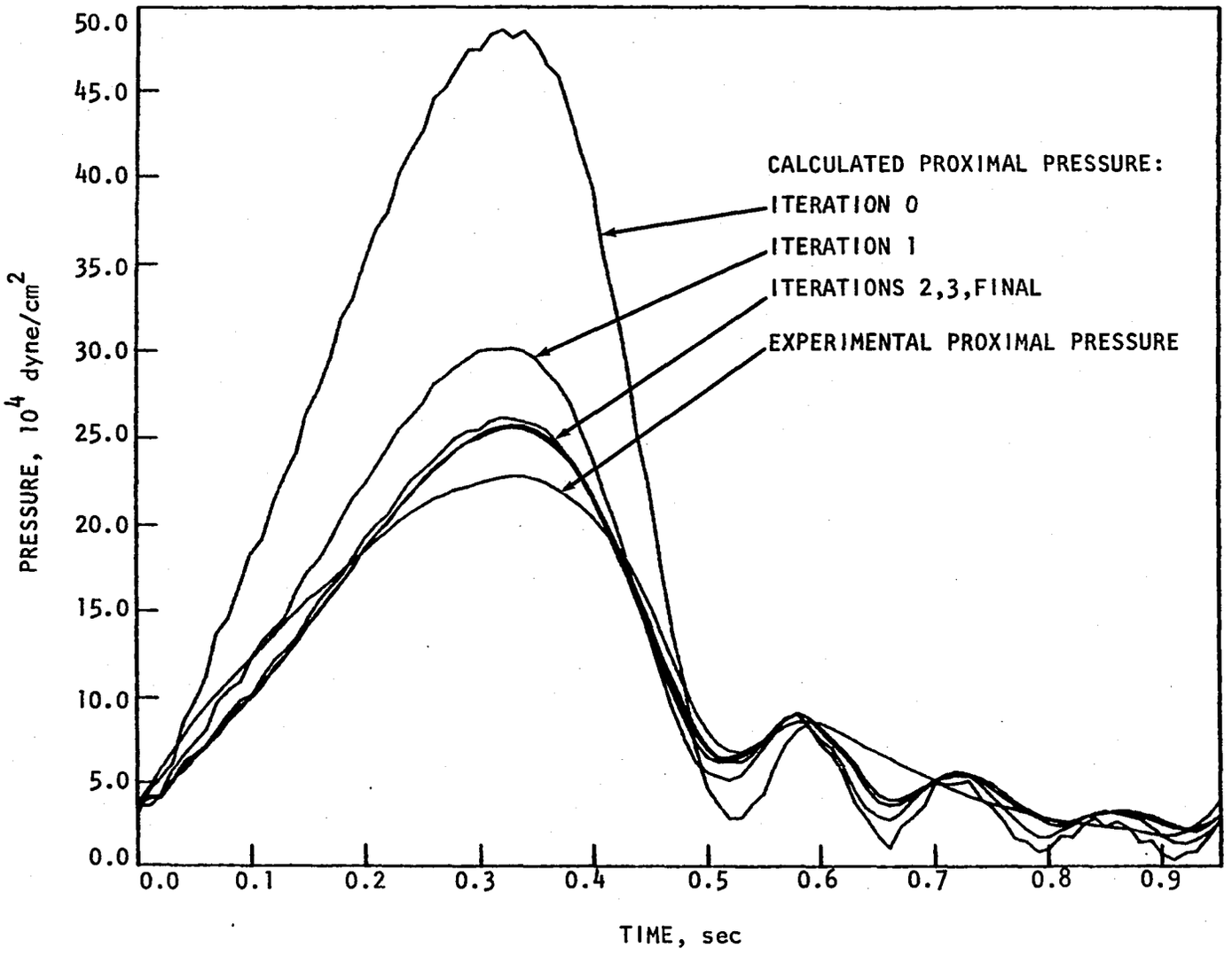
50.0
45.0
40.0
35.0
30.0
25.0
20.0
15.0
10.0
5.0
0.0
PRESSURE, 10^4 dyne/cm^2
0.0
0.1
0.2
0.3
0.4
0.5
0.6
0.7
0.8
0.9
TIME, sec
CALCULATED PROXIMAL PRESSURE:
ITERATION 0
ITERATION 1
ITERATIONS 2,3,FINAL
EXPERIMENTAL PROXIMAL PRESSURE

Figure 6.17. Convergence of calculated distal flow waveforms from parameter estimation trial. Branched tube with 90% stenosis upstream from branch

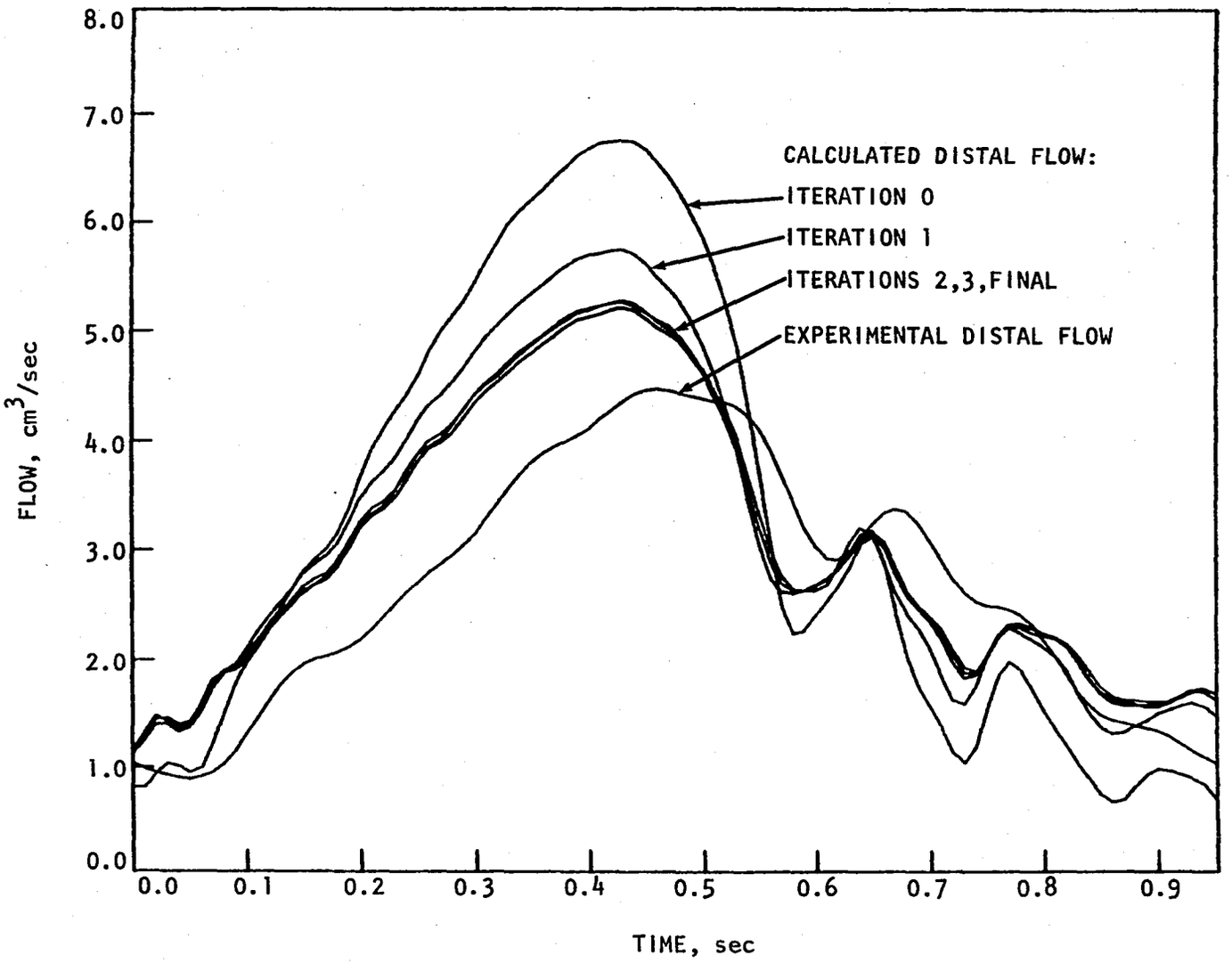
8.0
7.0
6.0
5.0
4.0
3.0
2.0
1.0
0.0
FLOW, cm³/sec
0.0
0.1
0.2
0.3
0.4
0.5
0.6
0.7
0.8
0.9
TIME, sec
CALCULATED DISTAL FLOW:
ITERATION 0
ITERATION 1
ITERATIONS 2,3,FINAL
EXPERIMENTAL DISTAL FLOW

CHAPTER 7

DISCUSSION AND SUMMARY

The mathematical model in conjunction with the finite element numerical scheme provided pressure and flow waveforms which matched satisfactorily with those obtained experimentally. The major sources of modeling error were attributed to the assumptions of constant compliance and resistance and to the use of a coarse finite element mesh in the numerical solution scheme. Other factors were errors in the experimental data and errors induced by the simple branch model. The computed pressures and flows were sensitive to variations in the vessel compliance, the peripheral resistance, and the severity and location of a stenosis. However, there was no appreciable sensitivity to variations of the vessel radius.

The finite element method provided a versatile means of representing the model equations in a form suitable for numerical integration. However, the integration procedure was not efficient with regard to computation requirements. For example, the numerical solution of the branch model equations required approximately four minutes of CPU time on a digital computer (DEC-VAX) if 24 nodes were incorporated into the finite element discretization. While this is not excessive for a simple modeling application, many iterations may be required in the parameter estimation scheme.

The parameter estimation provided reliable values for the vessel compliance, peripheral resistance, and location and severity of a stenosis independent of initial parameter values. The parameter

estimation technique appeared to be satisfactory since model-to-model comparisons produced very accurate estimates. Therefore, discrepancies between the estimated parameters and parameters measured directly are thought to be caused by modeling errors and inaccuracies in the physical measurements.

The main purpose of this dissertation, which was to provide an assessment of the applicability of parameter estimation to the evaluation of arterial parameters, has thus been fulfilled. However, questions have arisen which provide the basis for future research. First, the mathematical model may require modification to include such effects as vessel taper and nonlinear compliance in order to represent physiological data faithfully. Also, additional study of the effects of branching flow followed by possible modification of the branch equations is suggested.

Continued development of data acquisition and processing techniques is also a prime concern. Noninvasive measurement devices which provide accurate data with minimal difficulty are required to apply the estimation techniques in a clinical environment.

Additional research directed toward the application of estimation techniques should include the development of a more efficient numerical scheme. For example, finite element discretization of both the spatial and time dependence may reduce computation time. Investigation of the effects of noise and measurement error upon estimated parameter values is warranted if estimation techniques are to be applied to <u>in vivo</u> data.

Improvements in the mathematical model will probably require additional characteristic parameters. This raises the question of how many

parameters can be accurately estimated using the available data. The answer to this question may require that other estimation algorithms be tested if, for example, important parameters exhibit low sensitivity. In addition, since initial parameter values are generally not known *a priori*, an important result would be the determination of the regions of convergence for the parameters of interest.

In conclusion, the concepts detailed in this dissertation offer great promise to cardiovascular research. Parameter estimation methods yield information which can provide a better understanding of the factors which affect the circulation. Of greater importance, however, is the potential use of modeling and estimation techniques to provide clincial assessment of arterial disease. It is believed that the results of this dissertation support the feasibility of using these techniques as a diagnostic tool and further research is warranted.

REFERENCES

Anliker, M., R. L. Rockwell and E. Ogden. 1971a. Nonlinear analysis of flow pulses and shock waves in arteries: I. Derivation and properties of mathematical model. Zeitschrift für Angewandte Mathematik und Physik 22:217-246.

Anliker, M., R. L. Rockwell and E. Ogden. 1971b. Nonlinear analysis of flow pulses and shock waves in arteries: II. Parametric study related to clinical problems. Zeitschrift für Angewandte Mathematik und Physik 22:563-581.

Anliker, M., J. C. Stettler, P. Niederer and R. Holenstein. 1978. Prediction of shape changes of propagating flow and pressure pulses in human arteries. Pages 15-34 in R. D. Bauer and R. Busse, eds. The arterial system: dynamics, control theory and regulation. Springer-Verlag, Berlin.

Attinger, E. O. 1964. Flow patterns and vascular geometry. Pages 179-200 in E. O. Attinger, ed. Pulsatile blood flow. McGraw-Hill, New York.

Bard, Y. 1974. Nonlinear parameter estimation. Academic Press, New York.

Beck, J. V. and K. J. Arnold. 1977. Parameter estimation in engineering and science. John Wiley and Sons, New York.

Bekey, G. A. and S. M. Yamashiro. 1976. Parameter estimation in mathematical models of biological systems. Advances in Biomedical Engineering 6:1-43.

Beneken, J. E. W. 1972. Some computer models in cardiovascular research. Pages 173-223 in D. H. Bergel, ed. Cardiovascular fluid dynamics, Volume I. Academic Press, London.

Bourne, P. R. and R. I. Kitney. 1978. Matching techniques for clinical models of the circulation. Medical and Biological Engineering and Computing 16:689-696.

Brech, R. and B. J. Bellhouse. 1973. Flow in branching vessels. Cardiovascular Research 7:593-600.

Chang, P. P., G. L. Matson, J. E. Kendrick and V. C. Rideout. 1974. Parameter estimation in the canine cardiovascular system. IEEE Transactions on Automatic Control AC-19:927-931.

Christiansen, J. 1970. Numerical solution of ordinary simultaneous differential equations of the 1st order using a method for automatic step change. Numerische Mathematik 14:317-324.

Clark, C. 1976a. The fluid mechanics of aortic stenosis: I. Theory and steady flow experiments. Journal of Biomechanics 9:521-528.

Clark, C. 1976b. The fluid mechanics of aortic stenosis: II. Unsteady flow experiments. Journal of Biomechanics 9:567-573.

Clark, J. W., Jr., R. Y. S. Ling, R. Srinivasan, J. S. Cole and R. C. Pruitt. 1980. A two-stage identification scheme for the determination of the parameters of a model of left heart and systemic circulation. IEEE Transactions on Biomedical Engineering BME-27:20-29.

Crowe, W. J., Jr. and L. J. Krovetz. 1972. Studies of arterial branching in models using flow birefringence. Medical and Biological Engineering 10:415-426.

Dennison, J. C., J. H. Christian and D. E. Dick. 1972. Cardiovascular parameter estimation. Biomedical Sciences Instrumentation 9:89-94.

Desai, C. S. and J. F. Abel. 1972. Introduction to the finite element method: a numerical method for engineering analysis. Van Nostrand Reinhold Company, New York.

Greene, F. M., G. Fell and D. E. Strandness. 1980. Computer analysis of carotid arterial disease. Page 94 in Proceedings of the 33rd Annual Conference for Engineering in Medicine and Biology, Washington, D. C.

Holenstein, R. and P. Niederer. 1980. Propagation and damping of flow and pressure pulses in the human arterial tree. Pages 315-328 in Proceedings of the International Conference on Finite Elements in Biomechanics, February 18-20, 1980 in Tuscon, Arizona.

Kandarpa, K. and N. Davids. 1976. Analysis of the fluid dynamic effects on atherogenesis at branching sites. Journal of Biomechanics 9: 735-741.

McDonald, D. A. 1974. Blood flow in arteries. 2nd Edition. The Williams and Wilkins Company, Baltimore.

Newman, D. L., N. Waterhof and P. Sipkema. 1979. Modelling of aortic stenosis. Journal of Biomechanics 12:229-235.

Noordergraaf, A. 1978. Circulatory system dynamics. Academic Press, New York.

Noordergraaf, A., P. D. Verdouw, A. G. N. von Brummelen and F. W. Wiegel. 1964. Analog of the arterial bed. Pages 373-388 in E. O. Attinger, ed. Pulsatile blood flow. McGraw-Hill, New York.

Olsen, J. H. and A. H. Shapiro. 1967. Large-amplitude unsteady flow in liquid-filled elastic tubes. Journal of Fluid Mechanics 29:513-538.

Patel, D. J., J. C. Greenfield, Jr. and D. L. Fry. 1964. In vivo pressure-length-radius relationship of certain blood vessels in man and dog. Pages 293-305 in E. O. Attinger, ed. Pulsatile blood flow. McGraw-Hill, New York.

Raines, J. K., M. Y. Jaffrin and A. H. Shapiro. 1974. A computer simulation of arterial dynamics in the human leg. Journal of Biomechanics 7:77-91.

Rideout. V. C. and J. E. W. Beneken. 1975. Parameter estimation applied to physiological systems. Proceedings of the International Association for Analog Computation 17:23-36.

Rooz, E. 1980. A finite element simulation of pulsatile flow in flexible tubes. Ph.D. Thesis. Iowa State University, Ames.

Rumberger, J. A. and R. M. Nerem. 1977. A method-of-characteristics calculation of coronary blood flow. Journal of Fluid Mechanics 32: 429-448.

Schaaf, B. W. and P. H. Abbrecht. 1972. Digital computer simulation of human systemic arterial pulse wave transmission: a nonlinear model. Journal of Biomechanics 5:345-364.

Seeley, B. D. and D. F. Young. 1976. Effect of geometry on pressure losses across models of arterial stenoses. Journal of Biomechanics 9:439-448.

Simon, B. R., ed. 1975. The IMSL Library Edition 5. International Mathematical and Statistical Libraries, Inc., Houston.

Sims, J. B. 1972. Estimation of arterial system parameters from dynamic records. Computers and Biomedical Research 5:131-147.

Skalak, R. 1972. Synthesis of a complete circulation. Pages 341-376 in D. H. Bergel, ed. Cardiovascular fluid dynamics: Volume 2. Academic Press, New York.

Skalak, R. and T. C. Stathis. 1966. A porous tapered elastic tybe model. Pages 68-81 in Y. C. Fung, ed. Biomechanics. American Society of Mechanical Engineers, New York.

Snyder. M. F. and V. C. Rideout. 1968. Computer modeling of the human systemic arterial tree. Journal of Biomechanics 1:341-353.

Strano, J. J. 1973. Determination of in vivo human aorta parameters. 26th Annual Conference for Engineering in Medicine and Biology, Arlington, Virginia, page 111.

Streeter, V. L., W. F. Keitzer and D. F. Bohr. 1963. Pulsatile pressure and flow through distensible vessels. Circulation Research 13:3-20.

Taylor. M. G. 1965. Wave travel in a non-uniform transmission line, in relation to pulses in arteries. Physics in Medicine and Biology 10: 539-550.

Vander Werff, T. J. 1974. Significant parameters in arterial pressure and velocity development. Journal of Biomechanics 7:437-447.

Welkowitz, W. 1977. Engineering hemodynamics: applications to cardiac assist devices. D. C. Heath and Company, Lexington, Massachusetts.

Welkowitz, W., S. Fich and J. J. Strano. 1972. Cost function analysis applied to the determination of aorta parameters. International Journal of Engineering Science 10:1081-1091.

Wemple, R. R. and L. F. Mockros. 1972. Pressure and flow in the systemic arterial system. Journal of Biomechanics 5:629-641.

Wesseling, K. H., B. deWit and J. E. W. Beneken. 1973. Arterial haemodynamic parameters derived from noninvasively recorded pulsewaves using parameter estimation. Medical and Biological Engineering 11: 724-731.

Westerhof, N., F. Bosman, C. J. DeVries and A. Noordergraaf. 1969. Analog studies of the human systemic arterial tree. Journal of Biomechanics 2:121-143.

Westerhof, N. and A. Noordergraaf. 1970. Arterial viscoelasticity: a generalized model: effect on input impedance and wave travel in the systemic tree. Journal of Biomechanics 3:357-379.

Young, D. F. 1979. Fluid mechanics of arterial stenoses. Journal of Biomedical Engineering 101:157-175.

Young, D. F., N. R. Cholvin and A. C. Roth. 1975. Pressure drop across artificially induced stenoses in the femoral arteries of dogs. Circulation Research 36:735-743.

Young, D. F., T. R. Rogge, T. A. Gray and E. Rooz. 1980. Indirect evaluation of system parameters for pulsatile flow in flexible tubes. To be published in Journal of Biomechanics.

Young, D. F. and F. Y. Tsai. 1973. Flow characteristics in models of arterial stenosis: II. Unsteady flow. Journal of Biomechanics 6: 547-559.

Zienkiewicz, O. C. 1977. The finite element method. McGraw-Hill Book Company, Ltd., London.

ACKNOWLEDGMENTS

I wish to express my appreciation to my co-major professors, Donald F. Young and Thomas R. Rogge, without whose patient guidance and counselling this dissertation would not have been possible. Additional thanks are due the remaining members of my graduate committee, Peter Colwell, Bruce R. Munson and Richard H. Pletcher.

APPENDIX A

The derivation of the finite element equations used in Chapter 3 is detailed in this section. Linear one-dimensional simplex elements are used and the Galerkin technique is employed to derive the element approximations (Zienkiewicz, 1977).

The straight tube element is shown in Figure A.1. The endpoints i and j of the element are called nodes and have global axial coordinates x_i and x_j, respectively. Linear shape functions (one-dimensional Hermite polynomials) $N_i(x)$ and $N_j(x)$ are defined for $x_i \leq x \leq x_j$ by

$$N_i(x) = \frac{x_j - x}{x_j - x_i}, \quad N_j(x) = \frac{x - x_i}{x_j - x_i} \tag{A.1}$$

so that $N_m(x_n) = \delta_{mn}$ (Kronecker-δ).

The linear approximation $Q^e(x,t)$ to the actual flow $Q(x,t)$ in the element which aggrees with $Q(x,t)$ at the nodes is

$$Q^e(x,t) = N_i(x)Q(x_i,t) + N_j(x)Q(x_j,t), \tag{A.2}$$

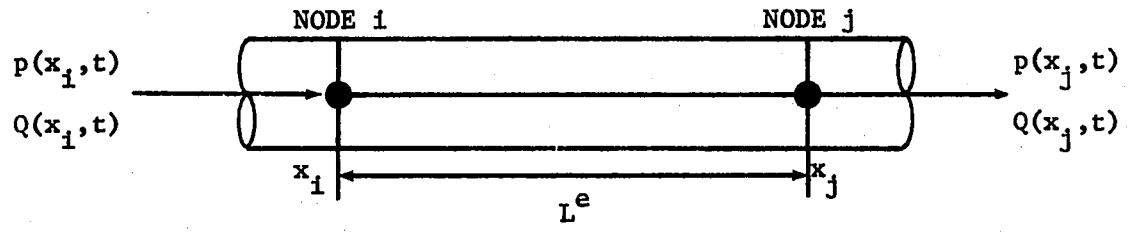

Figure A.1. Schematic diagram of straight tube element

or

$$Q^e = N_i Q_i + N_j Q_j \tag{A.3}$$

where, for example, the flow at node i is abbreviated $Q_i \equiv Q(x_i,t)$. The element interpolation for pressure is written similarly,

$$p^e = N_i p_i + N_j p_j. \tag{A.4}$$

Equations A.3 and A.4 can be combined into the shorthand vector notation

$$\{Q^e, p^e\}^T = [N]\ \underline{\delta}^e \tag{A.5}$$

where

$$\underline{\delta}^e = \{Q_i,\ p_i,\ Q_j,\ p_j\}^T \tag{A.6}$$

is the element vector of nodal degrees of freedom and

$$[N] = \begin{pmatrix} N_i & 0 & N_j & 0 \\ 0 & N_i & 0 & N_j \end{pmatrix} \tag{A.7}$$

is the shape function matrix.

The linear interpolations represented by Equations A.3 and A.4 are inserted into the governing Equations 3.7 and 3.8 for a straight tube to yield

$$\frac{\partial Q^e}{\partial x} + C\frac{\partial p^e}{\partial t} = r_c \tag{A.8}$$

$$\frac{\partial p^e}{\partial x} + RQ^e + L\frac{\partial Q^e}{\partial t} = r_m\ . \tag{A.9}$$

The residuals r_c and r_m from the continuity and momentum equations, respectively, will not be zero, in general, since the element approximations Q^e and p^e are not solutions to the governing equations. Equations A.8 and A.9 may be combined in the form

$$\frac{\partial}{\partial x}\begin{Bmatrix} Q^e \\ p^e \end{Bmatrix} + \begin{bmatrix} 0 & 0 \\ R & 0 \end{bmatrix}\begin{Bmatrix} Q^e \\ p^e \end{Bmatrix} + \begin{bmatrix} 0 & L \\ C & 0 \end{bmatrix}\frac{\partial}{\partial t}\begin{Bmatrix} Q^e \\ p^e \end{Bmatrix} = \begin{Bmatrix} r_c \\ r_m \end{Bmatrix} \qquad (A.10)$$

or, using Equation A.5,

$$\frac{\partial}{\partial x}([N]\underline{\delta}^e) + \begin{bmatrix} 0 & 0 \\ R & 0 \end{bmatrix}[N]\underline{\delta}^e + \begin{bmatrix} 0 & C \\ L & 0 \end{bmatrix}\frac{\partial}{\partial t}([N]\underline{\delta}^e) = \underline{r}\,. \qquad (A.11)$$

Since the shape functions depend only upon axial position and the nodal degrees of freedom depend only upon time, Equation A.11 becomes

$$[N']\underline{\delta}^e + \begin{bmatrix} 0 & 0 \\ R & 0 \end{bmatrix}[N]\underline{\delta}^e + \begin{bmatrix} 0 & C \\ L & 0 \end{bmatrix}[N]\dot{\underline{\delta}}^e = \underline{r} \qquad (A.12)$$

where

$$[N'] = \frac{d}{dx}[N]\,, \quad \dot{\underline{\delta}}^e = \frac{d}{dt}\underline{\delta}^e. \qquad (A.13)$$

If $L^e = x_j - x_i$ represents the element length, then from Equation A.1,

$$N_i' = -\frac{1}{L^e}\,, \quad N_j' = \frac{1}{L^e} \qquad (A.14)$$

so that

$$[N'] = \begin{bmatrix} -\frac{1}{L^e} & 0 & \frac{1}{L^e} & 0 \\ 0 & -\frac{1}{L^e} & 0 & \frac{1}{L^e} \end{bmatrix}. \qquad (A.15)$$

The Galerkin technique is used to produce the finite element approximation by forcing the residual $\underline{r}$ to be orthogonal to the shape functions in the sense that

$$\int_{x_i}^{x_j} ([N]^T\underline{r})\,dx = \underline{0} \qquad (A.16)$$

where $\underline{0} = \{0, 0, 0, 0\}^T$. If the residual is replaced by the full expression in Equation A.12, this becomes

$$\int_{x_i}^{x_j} ([N]^T[N']\underline{\delta}^e + [N]^T\begin{bmatrix} 0 & 0 \\ R & 0 \end{bmatrix}[N]\underline{\delta}^e + [N]^T\begin{bmatrix} 0 & C \\ L & 0 \end{bmatrix}[N]\dot{\underline{\delta}}^e)\, dx = \underline{0} \tag{A.17}$$

or

$$[M]\dot{\underline{\delta}}^e + ([K_1] + [K_2])\underline{\delta}^e = \underline{0}\,. \tag{A.18}$$

The matrices [M], $[K_1]$ and $[K_2]$ are evaluated using the simplex integration formula

$$\int_{x_i}^{x_j} (N_i^m N_j^n)\, dx = \frac{m!n!L^e}{(m + n + 1)!} \tag{A.19}$$

(Zienkiewicz, 1977). The matrix [M] is computed as

$$[M] = \int_{x_i}^{x_j} ([N]^T\begin{bmatrix} 0 & C \\ L & 0 \end{bmatrix}[N])\, dx \tag{A.20}$$

$$= \int_{x_i}^{x_j} \begin{bmatrix} 0 & CN_i^2 & 0 & CN_iN_j \\ LN_i^2 & 0 & LN_iN_j & 0 \\ 0 & CN_iN_j & 0 & CN_j^2 \\ LN_iN_j & 0 & LN_j^2 & 0 \end{bmatrix} dx. \tag{A.21}$$

Equation A.19 is applied to this expression to yield

$$[M] = \begin{pmatrix} 0 & \frac{CL^e}{3} & 0 & \frac{CL^e}{6} \\ \frac{LL^e}{3} & 0 & \frac{LL^e}{6} & 0 \\ 0 & \frac{CL^e}{6} & 0 & \frac{CL^e}{3} \\ \frac{LL^e}{6} & 0 & \frac{LL^e}{3} & 0 \end{pmatrix}. \tag{A.22}$$

Next, $[K_1]$ is evaluated:

$$[K_1] = \int_{x_i}^{x_j} ([N]^T[N']) \, dx \tag{A.23}$$

$$= \int_{x_i}^{x_j} \begin{pmatrix} -\frac{N_i}{L^e} & 0 & \frac{N_i}{L^e} & 0 \\ 0 & -\frac{N_i}{L^e} & 0 & \frac{N_i}{L^e} \\ -\frac{N_i}{L^e} & 0 & \frac{N_i}{L^e} & 0 \\ 0 & -\frac{N_i}{L^e} & 0 & \frac{N_i}{L^e} \end{pmatrix} dx. \tag{A.24}$$

Equation A.19 is used to evaluate the integral to provide

$$[K_1] = \begin{pmatrix} -\frac{1}{2} & 0 & \frac{1}{2} & 0 \\ 0 & -\frac{1}{2} & 0 & \frac{1}{2} \\ -\frac{1}{2} & 0 & \frac{1}{2} & 0 \\ 0 & -\frac{1}{2} & 0 & \frac{1}{2} \end{pmatrix}. \tag{A.25}$$

Finally, the matrix $[K_2]$ is calculated as follows:

$$[K_2] = \int_{x_i}^{x_j} ([N]^T \begin{pmatrix} 0 & 0 \\ R & 0 \end{pmatrix} [N])\, dx \tag{A.26}$$

$$= \int_{x_i}^{x_j} \begin{pmatrix} 0 & 0 & 0 & 0 \\ RN_i^2 & 0 & RN_iN_j & 0 \\ 0 & 0 & 0 & 0 \\ RN_iN_j & 0 & RN_j^2 & 0 \end{pmatrix} dx. \tag{A.27}$$

This integral is computed using Equation A.19,

$$[K_2] = \begin{pmatrix} 0 & 0 & 0 & 0 \\ \frac{RL^e}{3} & 0 & \frac{RL^e}{6} & 0 \\ 0 & 0 & 0 & 0 \\ \frac{RL^e}{6} & 0 & \frac{RL^e}{3} & 0 \end{pmatrix}. \tag{A.28}$$

The results of Equations A.22, A.25 and A.28 are inserted into Equation A.18 to derive the element equations

$$\begin{pmatrix} 0 & \frac{CL^e}{3} & 0 & \frac{CL^e}{6} \\ \frac{LL^e}{3} & 0 & \frac{LL^e}{6} & 0 \\ 0 & \frac{CL^e}{6} & 0 & \frac{CL^e}{3} \\ \frac{LL^e}{6} & 0 & \frac{LL^e}{3} & 0 \end{pmatrix} \underline{\dot{\delta}}^e + \begin{pmatrix} -\frac{1}{2} & 0 & \frac{1}{2} & 0 \\ \frac{RL^e}{3} & -\frac{1}{2} & \frac{RL^e}{6} & \frac{1}{2} \\ -\frac{1}{2} & 0 & \frac{1}{2} & 0 \\ \frac{RL^e}{6} & -\frac{1}{2} & \frac{RL^e}{3} & \frac{1}{2} \end{pmatrix} \underline{\delta}^e$$

$$= \underline{0}. \tag{A.29}$$

In order to apply the numerical integration scheme which was chosen to solve the finite element equations, it is necessary to have Equation A.29 be expressed in the form

$$\dot{\underline{\delta}}^e = [K^e]\underline{\delta}^e. \tag{A.30}$$

Evidently $[K^e] = [M]^{-1}([K_1] + [K_2])$. The inverse of [M] is computed as

$$[M]^{-1} = \begin{pmatrix} 0 & \frac{4}{LL^e} & 0 & -\frac{2}{LL^e} \\ \frac{4}{CL^e} & 0 & -\frac{2}{CL^e} & 0 \\ 0 & -\frac{2}{LL^e} & 0 & \frac{4}{LL^e} \\ -\frac{2}{CL^e} & 0 & \frac{4}{CL^e} & 0 \end{pmatrix}. \tag{A.31}$$

Therefore, $[K^e]$ is the matrix

$$[K^e] = \begin{pmatrix} -\frac{R}{L} & \frac{1}{LL^e} & 0 & -\frac{1}{LL^e} \\ \frac{1}{CL^e} & 0 & -\frac{1}{CL^e} & 0 \\ 0 & \frac{1}{LL^e} & -\frac{R}{L} & -\frac{1}{LL^e} \\ \frac{1}{CL^e} & 0 & -\frac{1}{CL^e} & 0 \end{pmatrix}. \tag{A.32}$$

Finally, Equation A.30 can be rewritten using Equation A.32 and Equation A.6 to express the nodal equations individually as

$$\dot{Q}_i = -\frac{R}{L} Q_i + \frac{1}{LL^e}(p_i - p_j) \tag{A.33}$$

$$\dot{p}_i = \frac{1}{CL^e}(Q_i - Q_j) \tag{A.34}$$

$$\dot{Q}_j = -\frac{R}{L} Q_j + \frac{1}{LL^e}(p_i - p_j) \tag{A.35}$$

$$\dot{p}_j = \frac{1}{CL^e}(Q_i - Q_j). \tag{A.36}$$

Equations A.33 through A.36 are the element equations presented in Chapter 3 as Equations 3.17 through 3.20.

APPENDIX B

Details of the development of the Gauss-Newton minimization algorithm used in the parameter estimation procedure of Chapter 5 will be presented in this section. This algorithm is used to minimize a sum of squares error function.

Let $\underline{Y}$ represent a measured data vector with N components and let $\underline{y}(\underline{b})$ denote the corresponding model vector calculated using the M-dimensional vector $\underline{b}$ of parameter values. The sum of squared error S between measured and calculated data can be written in the equivalent forms

$$S = (\underline{Y} - \underline{y}(\underline{b}))^T(\underline{Y} - \underline{y}(\underline{b})) \equiv \sum_{i=1}^{n} (Y_i - y_i(\underline{b}))^2 \tag{B.1}$$

where T means transpose. In order to minimize S with respect to the parameter vector $\underline{b}$, a necessary condition is that the partial derivatives of S with respect to the components b_j of $\underline{b}$ vanish at the critical values $\underline{b}^*$. That is,

$$\frac{\partial S}{\partial b_j}\bigg|_{\underline{b} = \underline{b}^*} = 0, \quad j = 1, 2, \ldots, M. \tag{B.2}$$

Differentiating Equation B.1 with respect to b_j and setting the result equal to zero yields

$$\frac{\partial S}{\partial b_j} = -2\left(\frac{\partial \underline{y}(\underline{b}^*)}{\partial b_j}\right)^T(\underline{Y} - \underline{y}(\underline{b}^*)) = 0 \tag{B.3}$$

or equivalently,

$$\left(\frac{\partial \underline{y}(\underline{b}^*)}{\partial b_j}\right)^T(\underline{Y} - \underline{y}(\underline{b}^*)) = 0. \tag{B.4}$$

The matrix $[X(\underline{b})]$ of sensitivity coefficients is defined as

$$X_{ij}(\underline{b}) = \frac{\partial y_i(\underline{b})}{\partial b_j}, \quad i = 1, 2, \ldots, N; \quad j = 1, 2, \ldots, M. \tag{B.5}$$

Equation B.4 can then be written in the form

$$[X(\underline{b}^*)]^T(\underline{Y} - \underline{y}(\underline{b}^*)) = \underline{0} \tag{B.6}$$

where $\underline{0}$ is the M-dimensional zero vector.

In general, $\underline{y}(\underline{b})$ will depend implicitly upon the parameters $\underline{b}$ so it is not possible to solve Equation B.6 for the critical values $\underline{b}^*$ directly. The purpose of the Gauss-Newton algorithm is to remedy this problem. Thus, assume that the components of $[X(\underline{b})]$ do not vanish in a neighborhood of $\underline{b}^*$ and let $\hat{\underline{b}}$ be any vector in that neighborhood. The Taylor series expansion of $\underline{y}$ about $\hat{\underline{b}}$ can be expressed as

$$\underline{y}(\underline{b}^*) = \underline{y}(\hat{\underline{b}}) + [X(\hat{\underline{b}})](\underline{b}^* - \underline{b}) + \ldots \tag{B.7}$$

where quadratic and higher order terms have been omitted.

To obtain the Gauss-Newton algorithm, two assumptions are made. First, $\underline{y}(\underline{b}^*)$ is assumed to be approximately equal to the linear terms in Equation B.7. Second, it is assumed that $[X(\underline{b}^*)]$ is approximately equal to $[X(\hat{\underline{b}})]$. With these two simplifications, Equation B.6 is represented by the approximation

$$[X(\hat{\underline{b}})]^T(\underline{Y} - \underline{y}(\hat{\underline{b}}) - [X(\hat{\underline{b}})](\underline{b}^* - \hat{\underline{b}})) = \underline{0}. \tag{B.8}$$

If $\underline{y}$ is linear in the parameters $\underline{b}$ then Equation B.8 is exact. Since the critical parameters $\underline{b}^*$ appear explicitly, Equation B.8 can be solved for $\underline{b}^*$ directly to produce

$$\underline{b}^* = \hat{\underline{b}} + ([X(\hat{\underline{b}})]^T[X(\hat{\underline{b}})])^{-1}([X(\hat{\underline{b}})]^T(\underline{Y} - \underline{y}(\hat{\underline{b}})). \tag{B.9}$$

If $\underline{y}(\underline{b})$ is nonlinear in the parameters, then Equation B.8 is only an approximation and the result determined by Equation B.9 will not be the true critical parameter vector. However, if $\hat{\underline{b}}$ is sufficiently close to $\underline{b}^*$, then the result of Equation B.9 will be closer to the critical vector than was $\hat{\underline{b}}$ in the sense that the sum of squares S will be reduced. Thus, an iterative procedure can be formulated as follows. Let $\underline{b}^{(k+1)} = \underline{b}^*$, $\underline{b}^{(k)} = \hat{\underline{b}}$, $[X^{(k)}] = [X(\hat{\underline{b}})]$ and $\underline{y}^{(k)} = \underline{y}(\hat{\underline{b}})$. Then Equation B.9 can be expressed as

$$\underline{b}^{(k+1)} = \underline{b}^{(k)} + ([X^{(k)}]^T[X^{(k)}])^{-1}([X^{(k)}]^T(\underline{Y} - \underline{y}^{(k)})) \qquad (B.10)$$

which is the Gauss-Newton algorithm. Since the right-hand side of Equation B.10 depends only upon the parameters $\underline{b}^{(k)}$, it may be used to determine an improved parameter vector from an initial estimate or guess which may subsequently be further improved by additional applications. Equation B.10 is the procedure presented as Equation 5.1 in Chapter 5.

APPENDIX C

Figure C.1. Experimental flexible tube test section

Figure C.2. Pressure transducer and electromagnetic flow probe

Figure C.3. In vitro experimental system